Asymmetry of both repressor and operator is important for the transcriptional regulation of the *P. putida* Xre-RES system

Frederik Oskar G. Henriksen, Ditlev E. Brodersen, and Ragnhild B. Skjerning[*]

Department of Molecular Biology and Genetics, Universitetsbyen 81, Aarhus University, DK-8000 Aarhus C, Denmark, [*]To whom correspondence should be addressed (raba@mbg.au.dk)

Keywords: Toxin-antitoxin; transcription; sigma 70; HTH domain; Cro repressor; NADase

ABSTRACT

Transcriptional regulation is a fundamental mechanism in bacteria and is often mediated by repressor proteins. In the type II toxin-antitoxin (TA) system. *xre-res*, the Xre antitoxin contains a putative helix-turn-helix (HTH) DNA-binding domain and could thus potentially bind to and repress transcription from the *xre-res* promoter. The structure of the *Pseudomonas putida* Xre-RES TA complex revealed an unusual 4:2 stoichiometry with two potential DNA-binding sites, suggesting a non-canonical mechanism of transcriptional autoregulation. Here, we show that the activity of the *xre-res* promoter requires both an intact σ^{70} element and the transcriptional start site, and that the Xre–RES complex represses transcription via binding to an imperfect inverted repeat region downstream of the σ^{70} element. We furthermore confirm the presence of the unusual 4:2 TA complex in solution and show that it preferably binds the imperfect inverted repeat in a 1:1 ratio. In addition, we show that the isolated Xre antitoxin is an aggregation-prone monomer *in vitro* and a weak repressor *in vivo.* We find that the Xre dimer can dissociates within the 4:2 complex and result in a 2:2 TA complex that still neutralizes the RES toxin but cannot bind DNA. Together, our data suggests that the asymmetry of the promoter is important for both transcription and repression, and we propose a model in which the Xre-RES complex regulates transcription through a dynamic and concentration-dependent equilibrium between a non-binding (2:2) and a DNA-binding (4:2) form.

33 **IMPORTANCE**

34 Transcriptional regulation is fundamental for bacteria to survive in a constantly changing
35 environment and requires the RNA polymerase, which recognizes and binds to a DNA element (the
36 promoter) located upstream of the gene and initiates transcription. Transcriptional repressors can
37 bind DNA and inhibit transcription by the RNA polymerase, but the exact recognition of DNA
38 binding sites remains unclear. The Xre antitoxin from the *Pseudomonas putida* toxin-antitoxin
39 system Xre-RES contains a putative DNA-binding domain, and the unusual ratio of antitoxin to
40 toxin within the protein complex suggests two potential DNA-binding sites. In this work, we show
41 that Xre-RES auto-regulates its own transcription through an asymmetrical DNA binding-site,
42 optimized to bind both the RNA polymerase and the Xre-RES complex, as well as a concentration-
43 dependent ratio of toxin to antitoxin within the complex. Our work provides insight on how
44 promoters can evolve to fine-tune the regulation of bacterial transcription.

45 **INTRODUCTION**

46 Regulation of transcription is a fundamental mechanism in bacteria that allows adaptation to
47 constantly changing environments, and RNA polymerase (RNAP) plays a central part in this. The
48 core RNAP enzyme has a $\beta\beta'\alpha_2$ subunit composition (1) but in order to form a holoenzyme and
49 initiate transcription at a particular promoter, the core enzyme needs to interact with a σ subunit (2,
50 3). The σ subunit ensures promoter recognition and positioning of the RNAP holoenzyme at the
51 promoter and unwinding of the DNA duplex near the transcriptional start site (TSS). Seven
52 different types of σ subunits have been identified in *E.coli*; σ^{70}, σ^{N} (σ^{54}), σ^{S} (σ^{38}), σ^{H} (σ^{32}), σ^{F} (σ^{28}),
53 σ^{E} (σ^{24}) and FecI (4). Most housekeeping genes expressed during exponential phase growth are
54 transcribed by RNAP bound to σ^{70}, and the two principal elements for promoter recognition in this
55 case are the -10 (5'-TATAAT-3' consensus) and the -35 hexamers (5'-TTGACA-3' consensus) (2).
56

57 Transcriptional activity can also be modulated by repressor proteins that bind a segment of the
58 promoter (the operator) and inhibits transcription (5). Repression can occur by one of three
59 mechanisms: steric hindrance of RNAP binding to the promoter, interference with post-recruitment
60 steps in transcriptional initiation such as the assembly of the RNAP holoenzyme, or DNA looping
61 upon repressor binding (1). A common DNA-binding feature of many repressor proteins is the
62 helix-turn-helix (HTH) domain (6). The basic HTH domain consists of three core helices making up
63 a right-handed helical bundle with a partly open configuration, where typically two HTH domains
64 are used to recognise the operator containing inverted or direct repeat sequence elements. The
65 efficiency of binding of a repressor protein to an operator site depends on its binding affinity, which
66 again is determined by base-specific readouts and intrinsic DNA shape, however, the exact
67 mechanism by with repressor proteins specifically recognise their DNA binding site(s) *in vivo*
68 remains unclear (7–9).

69

70 Due to the symmetrical nature of DNA, most protein repressors are functional as dimers, which
71 sometimes depend on even higher-order structures and additional proteins. In the widespread Xre-
72 RES system (10), the Xre (Xenobiotic Response Element) protein contains a putative HTH DNA-
73 binding domain that is stabilised in a higher-order structure through interaction with the associated
74 RES-domain protein (11–13). The two proteins are expressed from two-gene operons that have
75 been classified as toxin-antitoxin (TA) systems, which are widely distributed cellular regulators in
76 bacteria that encode a protein toxin that inhibits cell growth along with a cognate protein
77 antitoxin that neutralizes it (14). The RES toxin has an ADP-ribosyltransferase fold and
78 expression of a RES toxin from the insect pathogen *Photorhabdus luminescens* has been
79 shown to result in efficient depletion of intracellular NAD^+ in *E. coli*, suggesting that the RES
80 toxin is a NAD^+ glycohydrolase (NADase). Similar results were obtained for the RES-domain
81 toxins MbcT from *Mycobacterium tuberculosis* (12), SlvT from *P. putida* S12 (15), PA14_51010
82 from *P. aeruginosa* PA14 (16), and VPA0770 from *Vibrio parahaemolyticus* (17). Intriguingly, the
83 RES-domain toxin PrsT from *Sinorhizobium meliloti* toxin was found have the same fold but
84 functions as an ADP-ribosyltransferase (mART) targeting and inactivating phosphoribosyl
85 pyrophosphate synthetase (Prs), suggesting that the family is functionally diverse (13).

86

87 The crystal the structure of a Xre-RES complex from *Pseudomonas putida* revealed an unusual 4:2
88 TA stoichiometry in which each of the RES toxins of a central dimer interacts with a dimer of Xre
89 antitoxins, thus generating two potential DNA-binding HTH domains (11). The HTH domain of this
90 Xre antitoxin (Xre^{Pp}) is structurally similar to the bacteriophage lambda Cro repressor (18) and
91 could therefore potentially play a part in transcriptional regulation through binding of the
92 antitoxin to the TA promoter region, as observed for many TA systems (19). For some TA

93 systems, the presence of the toxin only stabilises the interaction with DNA up to a certain
94 level of stoichiometry after which further addition of toxin molecules leads to de-repression
95 by a mechanism that has been termed *conditional cooperativity* (20–22). However, other
96 modes of autoregulation exist, including recruitment of external regulators, three-component
97 TA systems for which the antitoxin itself lacks the DNA binding domain, and double
98 promoter mechanisms for TA modules with inversed gene order (23). The observation that
99 the *P. putida* Xre-RES complex contains two complete Cro-type DNA-binding domains
100 suggesting the system may be regulated in a novel way. However, the organisation of the
101 operator region as well as the mechanism of transcriptional regulation of this system is currently
102 unknown.
103
104 In this paper, we dissect the mechanism of transcriptional auto-regulation of the *P. putida xre-res*
105 system by first showing that the Xre–RES^{Pp} complex represses transcription via an imperfect
106 inverted repeat region downstream of the σ^{70} element. Moreover, we show that an intact σ^{70}
107 element, as well as the TSS, is required for the promoter to be active. We confirm that the 4:2
108 stoichiometry of the Xre-RES^{Pp} complex is present in solution and show that the complex
109 preferentially binds the imperfect inverted repeat region with high affinity in a 1:1 ratio. In addition,
110 we show that the isolated Xre antitoxin is a monomer *in vitro* and only weakly represses the
111 promoter *in vivo.* Surprisingly, the Xre^{Pp} dimer can dissociate within the 4:2 complex, which is in
112 an equilibrium with a 2:2 complex incapable of binding DNA. Together, our data suggest that the
113 promoter has evolved to efficiently bind both RNAP and the Xre^{Pp}–RES^{Pp} complex and we propose
114 a model for transcriptional autoregulation in which the complex exists in an equilibrium between a
115 non-binding 2:2 and a DNA-binding 4:2 form.
116

117 **RESULTS**

118 **The *P. putida xre-res* locus is transcriptionally auto-regulated**

119 The presence of an HTH DNA-binding domain in Xre^{Pp} strongly suggested that the antitoxin and/or
120 the Xre-RES TA complex could be involved in regulating transcription of the *P. putida xre-res*
121 operon via direct promoter binding. To understand if this is the case, we analysed the $xre\text{-}res^{Pp}$
122 promoter region (P_{XR}) and identified three inverted repeats and one directional repeat, two of which
123 overlap with a σ^{70} element (**Figure 1A and S1A**). To investigate the promoter activity *in vivo*, we
124 constructed a low-copy GFP reporter plasmid (pGH254Kgfp) containing the intact P_{XR} promoter
125 region, including the 5' end (30 bp) of xre^{Pp}, transcriptionally fused to *gfpmut2* encoding a Green
126 Fluorescent Protein (GFP) variant (S65A/V68L/S72A) with enhanced fluorescence emission and
127 more efficient folding at 37 °C as compared to the wild type GFP (24). This construct was then co-
128 transformed into *E. coli* MG1655 along with an arabinose-inducible plasmid containing the *xre-*
129 res^{Pp} operon and the GFP signal monitored throughout growth in the presence or absence inducer
130 (**Figure 1B**). The results show that the P_{XR} promoter region becomes increasingly active in *E. coli*
131 during exponential growth phase (**Figure 1C**, blue and orange curves), corresponding well with the
132 presence of a σ^{70} factor binding site in the promoter region that is known to be active during
133 exponential growth. Expression of $xre\text{-}res^{Pp}$ in this background results in complete absence of GFP
134 signal as controlled by the P_{XR} promoter (**Figure 1D**, orange curve) compared to the strain
135 containing an empty pBAD33 vector (**Figure 1D**, blue curve), indicating that $xre\text{-}res^{Pp}$ controls
136 expression from P_{XR}, possibly via binding of the $Xre\text{-}RES^{Pp}$ complex to DNA.

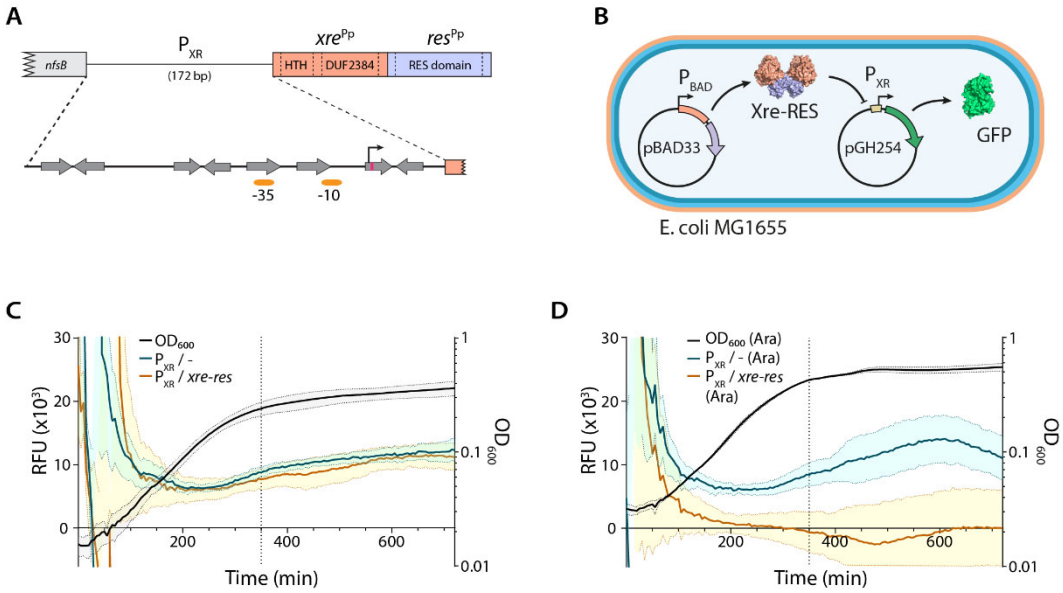

Figure 1. Organisation, activity, and regulation of the *xre*^{Pp}-*res*^{Pp} operon. **A.** Schematic representation the *xre-res*^{Pp} locus including the promoter region (P_{XR}) and the upstream gene (*nfsB*). Top, the *xre*^{Pp} gene (salmon) encodes a protein antitoxin with an N-terminal helix-turn-helix (HTH) domain and a C-terminal domain of unknown function (DUF2384), known to interact with the RES toxin, while *res*^{Pp} (blue) encodes a NADase toxin with a RES domain. Below, close-up of the P_{XR} promoter region upstream showing the three inverted repeats and one directional repeat (grey arrows), of which the last inverted repeat is imperfect and contains one mismatch (red box). The 5' end of *xre*^{Pp} (orange box), σ^{70} -35 and -10 promoter elements (orange ovals), and TSS (arrow) are indicated. **B**. Schematic representation of the experimental setup for the *in vivo* promoter activity assay. For pGH254Kgfp, the complete P_{XR} promoter region (**Figure S1A**, beige) was inserted upstream of *gfpmut2* (green), resulting in GFP being expressed when the promoter is active. For pBAD33, the *xre-res*^{Pp} genes (light red and light purple) were inserted downstream the arabinose inducible promoter P_{BAD}, and both plasmids were co-transformed into *E. coli* MG1655. **C** and **D.** Promoter activity measured as GFP relative fluorescence units (RFU) during growth without (C) or with (D) arabinose for *E. coli* MG1655 containing the promoter reporter pGH254Kgfp::P_{XR} (P_{XR}), as well as empty pBAD33 (-) or pBAD33::*xre*$_{naSD}$-*res*^{Pp} vector (*xre-res*). Curves show mean-of-mean values (line) with SEM (shadow). The dotted vertical line indicates the 350 min time point used in subsequent figures.

Transcription requires an intact σ^{70} element upstream of a *xre-res*^{Pp} operator site

To determine the minimal promoter requirements for active transcription from the *xre-res*^{Pp} locus, we repeated the promoter assay using variants of P_{XR} where one or more of the four identified repeats (S1-S4) were systematically removed (**Figure 2A** and **Table S3**). As the P_{XR} promoter was found to be most active during exponential growth, we decided to compare GFP fluorescence levels with and without expression of *xre-res*^{Pp} in the late-exponential growth phase (measured at t=350 min; complete curves are included in **Figure S1B-G**). Removal of S1 ($P_{XR}\Delta S1$) did not affect promoter activity, while removal both S1 and S2 ($P_{XR}\Delta S1$-S2), surprisingly, led to increased

promoter activity (**Figure 2B**). Conversely, removal of S1 through S3 (P_{XR}ΔS1-S3) or just S3 and S4 (P_{XR}ΔS3-4) completely abolished transcription, supporting the importance of the σ^{70} element mainly in S3 (**Figure 1A**). Deletion of S4 alone (P_{XR}Δ4), which would leave the -35 and -10 promoter elements intact, also abolished transcription, suggesting that an intact σ^{70} element and the TSS (+1), is required for transcription in this case. In line with this, removal of only the central palindromic part of the imperfect inverted repeat in S4 (P_{XR}Δrepeat, **Table S3**), which leaves the transcriptional start site intact, restored promoter activity to near-wild type levels (**Figure 2B**). Expression of *xre-res*^{Pp} led to complete transcriptional repression of all active promoter variants with the exception of the P_{XR}Δrepeat construct, for which only partly (and non-significant) repression was obtained (**Figure 2B**, Δrepeat). Taken together, the signals for transcription and regulation has been decoupled, showing that an intact σ^{70} element (from -35 to +1) is required for transcription and that *xre-res*^{Pp} represses the promoter via the imperfect inverted repeat in the S4 region.

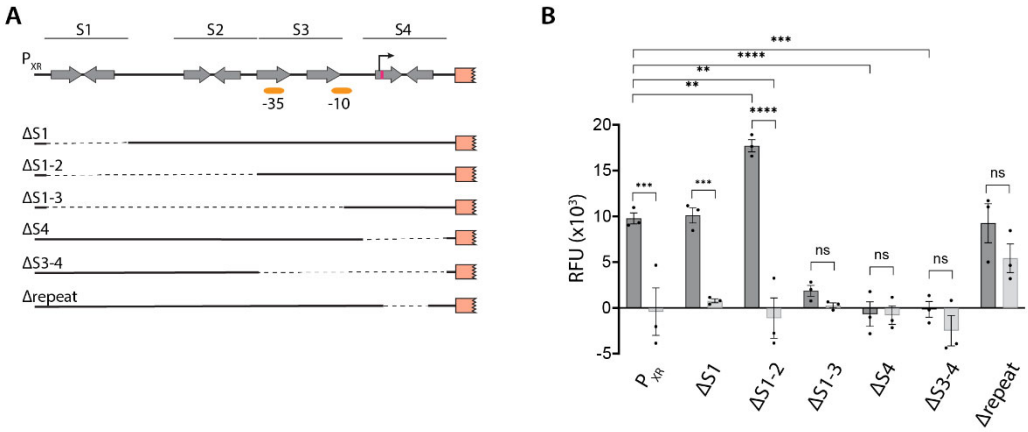

Figure 2. Determination of the minimal promoter requirements for transcription and regulation of P_{XR}. A. Detailed overview of the repetitive elements in P_{XR} and schematic representation of the designed promoter variants. The P_{XR} promoter, including the 5' end of *xre*^{Pp} (*xre*') consists of four regions (S1-S4), each covering one of the identified repeats. In the promoter variants below, full lines indicate the included parts while dotted lines represent regions that have been removed. Details of the constructs are found in **Table S1** and **Table S3**. **B.** Promoter activity assays in *E. coli* MG1655 containing the pGH254Kgfp reporter plasmid with the indicated promoter variations and pBAD33::*xre-res*^{Pp}. For each variant, the GFP fluorescence (RFU) measured at t=350 min from non-induced cultures (dark grey bars) is compared to that from arabinose-induced cultures (light gray bars). Mean RFU values extracted at the same time point from three independent experiments were treated as biological replicates (dots) and error bars show the standard error of the mean (SEM). Complete growth curves are included in **Figure S1**. *ns*, not significant; *, $p < 0.05$; **, $p < 0.01$; ***, $p < 0.01$; ****, $p < 0.0001$.

189

190 **The P_{XR} promoter likely evolved to balance RNA polymerase binding and *xre-res*^{Pp} regulation**

191 To gain a better understanding of how *xre-res*^{Pp} regulates its operator *in vivo*, we investigated how
192 the actual DNA sequence of the imperfect inverted repeat (S4) affects transcriptional repression
193 during late-exponential growth phase (using data at t=350 min; for complete curves see **Figure S2**).
194 First, we tested the importance of the imperfect inverted repeat by creating two corresponding
195 perfect inverted repeats by either introducing G->T on the coding strand in the first half of the
196 repeat (P_{XR}5'-perf) or A->C in the second half of the repeat (P_{XR}3'-perf) (**Figure 3A** and **Table S3**).
197 Both substitutions decreased promoter activity while neither of them affected the ability of *xre-res*^{Pp}
198 to control transcription, suggesting that the imperfect inverted repeat is required for optimal binding
199 of either the RNA polymerase or the σ^{70} factor itself to the promoter (**Figure 3B**). Next, we studied
200 the importance of the presence of an intact inverted repeat by changing 6-bp in either the first half
201 (P_{XR}5'-flip) or the second half of the repeat (P_{XR}3'-flip) to the corresponding reverse complement
202 sequences (**Figure 3A** and **Table S3**). Interestingly, alteration of the first half of the repeat
203 abolished promoter activity, while changes in the second half of the repeat did not affect
204 transcription to the same extent (**Figure 3B**). As the P_{XR}5'-flip variant alters the sequence at the
205 TSS, while the P_{XR}3'-flip leaves this sequence unaffected, this supports that the identity of the first
206 transcribed nucleotide is required for full promoter activity. Surprisingly, expression of *xre-res*^{Pp}
207 partly repressed promoter activity of the P_{XR}-3'-flip construct, indicating that an intact imperfect
208 inverted repeat is optimized, but not strictly required, for transcriptional regulation by *xre-res*^{Pp}.
209 Altogether, these data suggest that the P_{XR} promoter region, and in particular the imperfect inverted
210 repeat, has evolved to balance binding of the RNAP holoenzyme with regulation upon *xre-res*^{Pp}
211 expression.

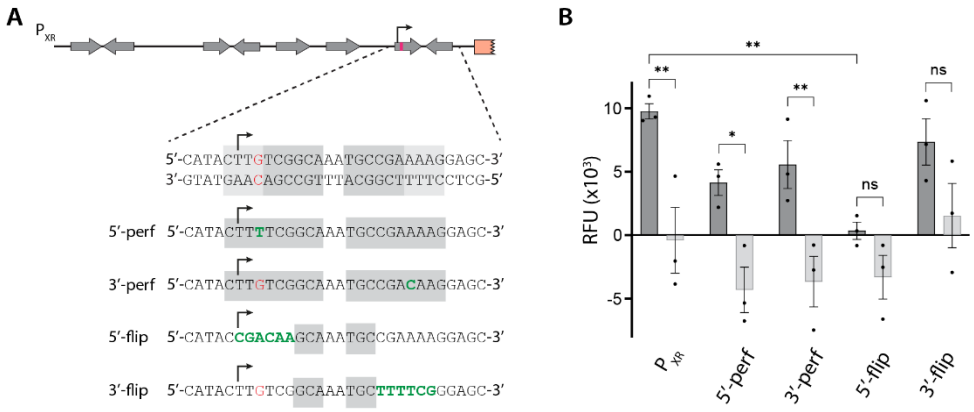

Figure 3. Functional analysis of the S4 repeat sequence. **A.** Schematic representation of the repeat variants of the imperfect inverted repeat in S4 of the P_{XR} promoter region. The DNA sequence of the imperfect inverted repeat is highlighted (light grey), including the mismatch in the first repeat (red), the perfect part (dark grey) and the alterations (green). The mismatch was removed by a substitution either in the first (5'-perf) or second (3'-perf) half of the repeat. Moreover, either the first half (5'-flip) or the second half of the repeat (3'-flip) were destroyed by reverse complementation of a 6-bp segment. The -35 and -10 promoter elements of the σ^{70} binding site are indicated with orange ovals and the TSS by a bent arrow. **B.** Promoter activity assays in *E. coli* MG1655 containing the pGH254Kgfp reporter plasmid with the indicated variations and pBAD33::xre^{Pp}_{naSD}-res^{Pp}. The relative fluorescence (RFU) measured from non-induced cultures (dark grey) of each promoter variant are shown next to values measured after arabinose-induction (light gray). Mean RFU values extracted at the same time point from three independent experiments were treated as biological replicates (dots) and error bars show the standard error of the mean (SEM). Complete growth curves are included in **Figure S1**. *ns*, not significant; *, $p < 0.05$; **, $p < 0.01$.

The Xre-RES^{Pp} complex binds directly to the imperfect inverted repeat in P_{XR} *in vitro*

The repression of transcription observed upon expression of *xre-res^{Pp}* suggested that the Xre-RES^{Pp} protein complex might binds directly to DNA via the HTH domains in Xre, as seen for many other types of type II toxin-antitoxin systems (19). To investigate this hypothesis, we analysed the binding between the protein complex and different parts of the P_{XR} promoter *in vitro*. First, we expressed and purified a Xre-RES^{Pp} complex via a N-terminal His_6-tag on the RES^{Pp} toxin (Xre-RES$^{Pp}_{His6}$) and used size exclusion chromatography coupled to multi-angle light scattering (SEC-MALS) to confirm that Xre and RES_{His6} form a protein complex with an estimated MW of 91.9 ± 4.2 kDa (**Figure 4A**), which corresponds well with a theoretical mass of the 4:2 complex of 102.84 kDa (**Figure 4B**). We then analysed the ability of the purified complex to bind 30 bp dsDNA probes corresponding to each of the sequence elements S1-S4 in the P_{XR} promoter (**Figure 1A** and **Figure S1A**). For this, purified Xre-RES$^{Pp}_{His6}$ complex hexamer and DNA duplex were incubated in a 1:1

239 molar ratio followed by analytical SEC (a-SEC). A change in elution volume of 0.2 mL and a
240 concomitant change in the 260/280 nm absorbance ratio from 0.54 to 0.68 was observed for
241 complex mixed with S4 dsDNA (Figure 4C), but not for S1, S2 or S3 dsDNA (**Figure S3A-C**),
242 suggesting that the Xre-RES^{Pp} complex binds specifically to the S4 element of the P_{XR} promoter.
243
244 Structural analysis of the 4:2 Xre-RES^{Pp} complex revealed two complete Cro-like Xre^{Pp} dimers
245 (11), each potentially capable of binding dsDNA via interaction with adjacent major grooves (25).
246 To investigate the binding stoichiometry of the observed *in vitro* interaction, we analysed the
247 binding at different protein:DNA ratios by a-SEC and SEC-MALS. At a 1:1 ratio of Xre-RES^{Pp}
248 complex to DNA, and thus a ratio of putative binding sites to DNA of 2:1, we found that the protein
249 complex was unable to bind all DNA present in solution (**Figure 4C**). To further probe the
250 stoichiometry of binding between the Xre-RES^{Pp} complex and S4 dsDNA, we saturated the protein
251 complex with increasing amounts of DNA and used high-resolution SEC to check for indication of
252 a second DNA binding site. At a 1:2 ratio of protein complex to DNA, no additional shift in the
253 elution volume was observed as compared to the 1:1 ratio of protein complex to DNA (**Figure**
254 **S3D**). Even at a ratio of protein to DNA of 1:10, only a marginal shift in the elution volume of 0.01
255 ml (0.6% CV) was observed (**Figure S3E**). Together, these data suggest that the 4:2 Xre-RES^{Pp}
256 complex, despite having two complete dsDNA binding sites, is only capable of binding a single
257 copy of S4 dsDNA.
258
259 To quantify the binding interaction between the Xre-RES^{Pp} complex and S4 as well as the variants
260 used in the promoter activity assays, we next determined the binding coefficient (K_D) using
261 isothermal titration calorimetry (ITC). This showed that the Xre-RES^{Pp} complex has a high affinity
262 towards the native S4 sequence (K_D = 231±46 nM, **Figure 4D**), while the affinities towards both the

263 5'-perf (K_D = 341 µM±264 µM) and 3'-perf variants (K_D = 80±79 µM) of S4 were drastically
264 reduced (**Table S4**). Surprisingly, ITC analysis of the 5'-flip and 3'-flip S4 variants did not show
265 any indications of binding, even when molar ratio of dsDNA to protein exceeded 3:1 (**Table S3**).
266 These results are thus in contrast to the *in vivo* assays (**Figure 3B**), in which expression of *xre-res*^{Pp}
267 partly represses promoter activity of the P_{XR}3'-flip construct, and suggest that repression of
268 transcription is either dependent on more than just binding of Xre-RES^{Pp} to S4 or that the conditions
269 within the cell are different from those *in vitro*.
270
271 In summary, we have confirmed the presence of the 4:2 Xre-RES^{Pp} complex, previously only
272 observed by x-ray crystallography, in solution. Moreover, our data show conclusively that Xre-
273 RES^{Pp} specifically binds the imperfect S4 repeat of the promoter in a 1:1 complex to DNA ratio and
274 that even single base changes in the repeat strongly reduces its binding affinity.

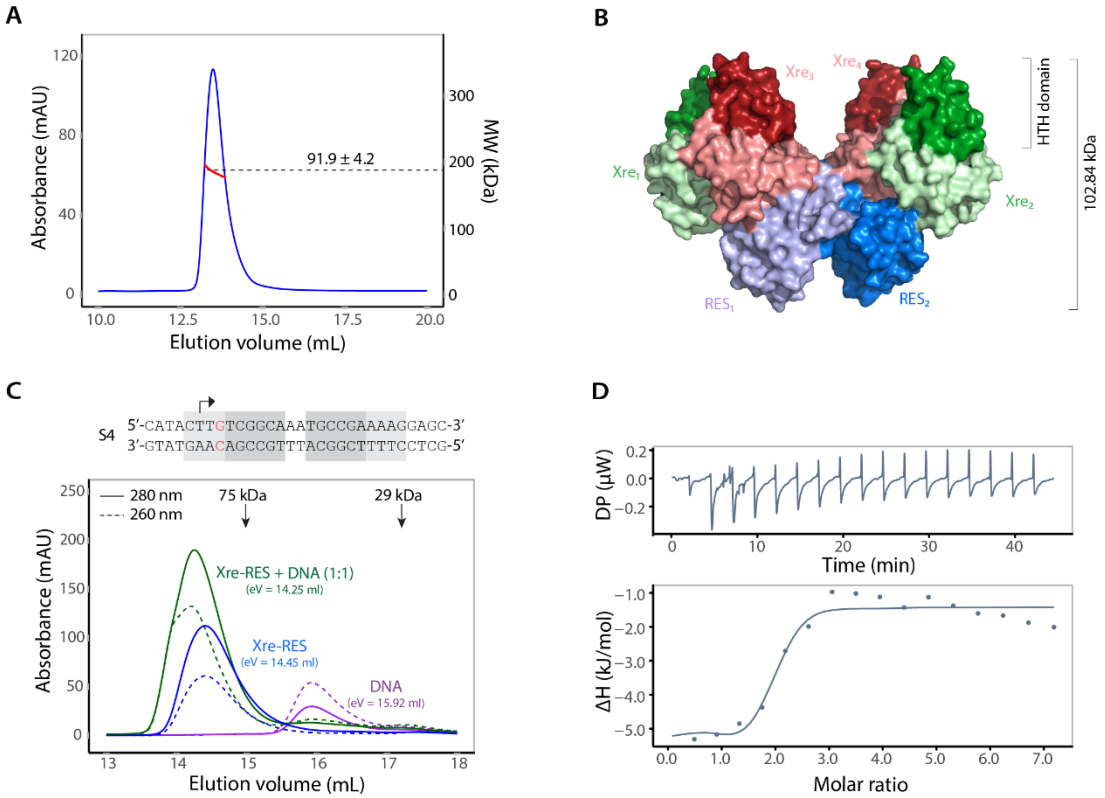

275
276 **Figure 4. Xre-RES^{Pp} forms a 4:2 hexameric complex in solution and interacts specifically with the S4**
277 **element of the promoter. A.** SEC-MALS analysis of purified Xre-RES$^{Pp}{}_{His6}$ complex. The chromatogram
278 shows the elution profile as measured by absorption at 280 nm (blue) and the molecular mass measured by

MALS (red). The average mass corresponding to the middle of the peak is 91.9 ± 4.2 kDa (dotted line). **B**. The crystal structure of heterohexameric Xre-RES^{Pp} (PDB: 6GW6) with total mass (102.84 kDa) and HTH domains indicated (11). The RES toxins are coloured in blue, while the Xre antitoxins are in light green and light red The HTH domains are in dark green and dark red. **C**. Analytical SEC (a-SEC) analysis of Xre-RES$^{Pp}_{His6}$ (Xre-RES, blue), S4 (DNA, purple), or DNA mixed with protein in a 1:1 ratio (Xre-RES + DNA, green). Elution volumes are noted. Black arrows represent known molecular weight standards (conalalbumin, 75 kDa; Carbonic anhydrase, 29 kDa). Full line shows 280 nm absorbance, while dotted line is 260 nm absorbance. **D**. Isothermal Titration Calorimetry (ITC) titration of S4 dsDNA into Xre-RES^{Pp} complex. The top panel shows the raw thermogram (DP, differential power), while the bottom panel shows the integrated heat per injection (ΔH), the solid is line is the fit using the "one set of sites" model.

The Xre^{Pp} dimer is stabilised by higher-order complex formation and required for transcriptional repression

Many type II TA systems rely on toxin:antitoxin complex formation in a certain ratio for the antitoxin to bind the promoter, and thereby repress transcription efficiently, and most often, the affinity of the isolated antitoxin for its operator site is relatively low (23). We therefore investigated whether transcriptional repression in the *xre-res*^{Pp} system could be achieved by expression of *xre*^{Pp} alone. First, we compared the activity of the wild type P_{XR} promoter during expression of either *xre*^{Pp} or *xre-res*^{Pp}. While expression of the complex fully repressed transcription, expression of *xre*^{Pp} alone only partially, and not significantly, repressed transcription (**Figure 5A**). Moreover, we note that the promoter activity between biological replicates was considerably more variable (**Figure S4**), potentially suggesting that *xre*^{Pp} is unstable when expressed without *res*^{Pp}.

The arrangement of the two adjacent HTH domains on the Xre^{Pp} dimer is remarkably similar to the structure of the Cro repressor bound to DNA (PDB: 1RPE) (**Figure 5B** and **5C**), suggesting that dimerisation is needed for efficient repression of transcription (11). The weak repression upon expression of isolated *xre*^{Pp} could thus be because it cannot form a stable dimer. To address this, we expressed and purified isolated Xre^{Pp} antitoxin with a C-terminal His-tag (Xre$^{Pp}_{CHis6}$) to avoid disturbing the dimerization interface. We noted that purified Xre$^{Pp}_{CHis6}$ protein was very prone to aggregation and could not be concentrated above 10 μM, suggesting that complex

309 formation is needed to stabilise the antitoxin. Moreover, the mass of purified Xre^{Pp}_{CHis6} antitoxin
310 was determined by SEC-MALS to be 22.2 ± 0.9 kDa, corresponding to a monomer of Xre^{Pp}
311 (**Figure 5D**). Complex formation thus appears needed for Xre^{Pp} to dimerise and thereby efficiently
312 repress transcription. In addition, we note that the structures of each Xre^{Pp} monomer in the dimer is
313 slightly different. The inner Xre^{Pp} monomers, which binds the RES toxin, are most similar to each
314 other with a C_α root mean square deviation (RMSD) of 1.044Å (149 to 149 atoms), while the outer
315 Xre^{Pp} monomers are less similar with an RMSD of 1.742Å (149 to 149 atoms) and this difference is
316 particularly pronounced in the HTH domain (**Figure 5E**). Thus, the DNA-binding domain of the
317 Xre^{Pp} is asymmetric, suggesting specific and directional binding of Xre-RES^{Pp} to S4.
318
319 The partial and variable repression by *xre*^{Pp} alone *in vivo*, together with the instability of isolated
320 Xre^{Pp} and detection of a monomer *in vitro*, suggests that that complex formation is needed to
321 stabilise Xre^{Pp}. We therefore investigated the stability the Xre^{Pp} dimer within the complex, using
322 mass photometry (MP) to determine the single-molecule mass of purified complex. Surprisingly,
323 the results revealed a concentration-dependent dissociation of the complex from 87±15 kDa to
324 54±14 kDa, which roughly corresponds to a transition from a 4:2 (103 kDa) to a 2:2 (69 kDa)
325 complex (**Figure 5F**). This shows that even within the complex, the Xre^{Pp} dimer is not stable and
326 suggests that the complex can exist in both a 2:2, 3:2 and 4:2 form.
327

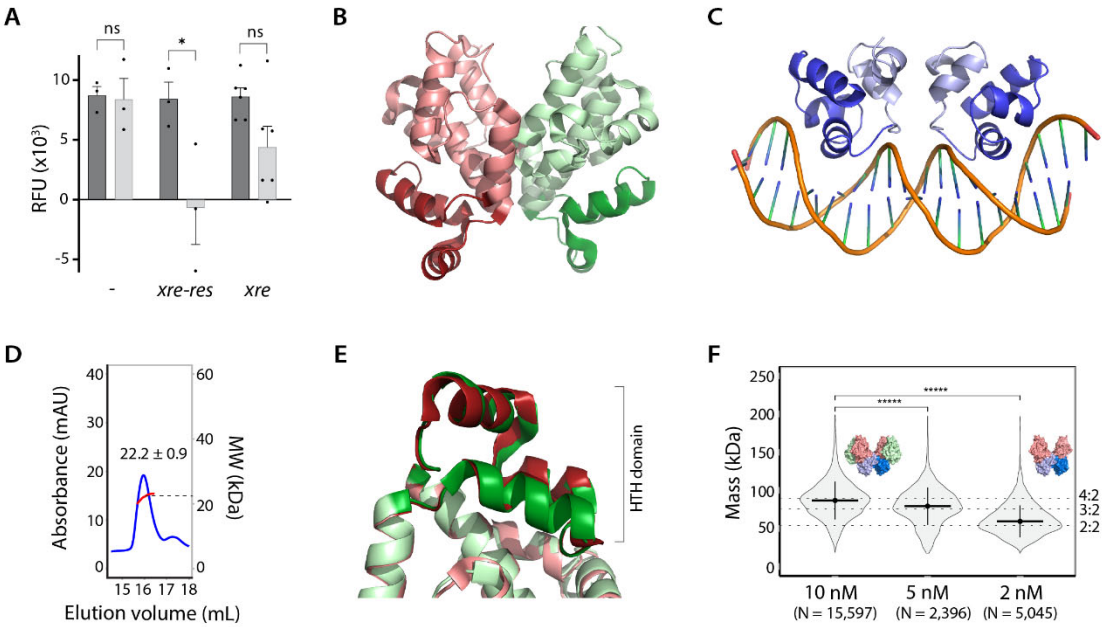

Figure 5. Isolated Xre^{Pp} is a monomer in solution and controls formation of a repressive 4:2 complex. **A**. Promoter activity assays in *E. coli* MG1655 containing the promoter reporter pGH254Kgfp::P_{XR} (P_{XR}), as well as empty pBAD33 (-), pBAD33::*xre*$_{opSD}$^{Pp} (*xre*), or pBAD33::*xre*$_{naSD}$-*res*^{Pp} vector (*xre-res*). The relative fluorescence (RFU) measured from non-induced (dark grey) cultures of each promoter variant were compared to those from arabinose-induced (light grey) cultures. Mean RFU values extracted at the same time point from three independent experiments were treated as biological replicates (dots) and error bars show the standard error of the mean (SEM). Complete growth curves are included in **Figure S4**. Mean values of relative fluorescence unit (RFU) for t=350 min were extracted independent experiments and treated as biological replicates (dots) for which error bars show the standard error of the mean (SEM). *ns*, not significant; *, $p < 0.05$. **B**. The structure of the Xre^{Pp} homodimer from the Xre-RES^{Pp} complex (PDB: 6HW6) (11). The HTH DNA-binding domain (residues 40-80) are shown in darker colors. **C**. The structure of bacteriophage Cro bound to DNA (PDB: 1RPE) (26). **D**. SEC-MALS analysis showing that isolated Xre^{Pp}$_{CHis6}$ is a monomer with a mass of 22.2 ±0.9 kDa in solution. The chromatogram shows elution profile measured by 280 nm absorbance (blue) and calculated mass from MALS (red). **E**. Structural overlay of the two Xre^{Pp} monomers from the homodimer (PDB: 6GW6) (11). The HTH DNA-binding domains are shown in darker colors. **E**. Single-molecule mass determination of Xre^{Pp}-RES^{Pp}$_{His6}$ at 2 nM (left), 5 nM (middle), and 10 nM (right). The violin plots show the density of all measured single-molecule events. The solid black horizontal line indicates the median mass, while the vertical line shows the standard deviation (SD). The theoretical masses of the Xre^{Pp}-RES^{Pp}$_{His6}$ complex with 4:2, 3:2, and 2:2 stoichiometries are indicated by dotted lines. Significance was tested with the Wilcoxon signed rank test. *****, p< 5.55e-7.

The rare tetrameric Xre-RES^{Pp} complex cannot bind DNA

The previously published structure of the Xre-RES^{Pp}$_{R23A}$ complex (11) shows that the N-terminus of Xre is important for antitoxin dimerisation. To confirm the existence of a 2:2 complex as proposed by mass photometry, we expressed and purified a variant of the Xre-RES^{Pp} complex with a N-terminal His$_6$-tag on Xre (Xre$_{NHis6}$-RES^{Pp}), which, based on the crystal structure, should prevent dimerisation. The expressed protein was highly prone to aggregation during purification, possibly

356 indicating a destabilised Xre^{Pp} dimer leading to free and unstable Xre^{Pp} monomers as well as a 2:2
357 complex. This was supported by SEC, which showed two peaks corresponding to the 2:2 complex
358 and isolated Xre^{Pp} antitoxin (**Figure S5A** and **S5B**). The isolation of a 2:2 complex was further
359 confirmed by mass photometry, where the main protein population at both 10 nM and 2 nM had a
360 mass of 63±18 kDa (**Figure 6A**), similar to the mass of the 4:2 complex at 2 nM concentration (55
361 ± 14 kDa).
362
363 As the isolated Xre^{Pp} antitoxin is a monomer and expression of *xre^{Pp}* alone only weakly represses
364 transcription *in vivo*, we predicted that the isolated 2:2 complex would have reduced DNA affinity.
365 As the expected elution volumes of the 2:2 complex and S4 dsDNA are very similar, we used a high-
366 resolution SEC column with a better length to bed-width ratio to maximize separation resolution, and
367 analysed samples containing DNA alone, 2:2 complex alone, or 2:2 complex to DNA in ratio of 1:10.
368 The resulting chromatograms showed that the elution volume of the 2:2 complex was not affected by
369 the addition of DNA (**Figure 6B**), which confirms that the 2:2 is a non-binding form of the Xre-
370 RES^{Pp} complex and supports a model in which the complex exists in a concentration-dependent
371 equilibrium between a non-binding (2:2) and DNA-binding (4:2) form.

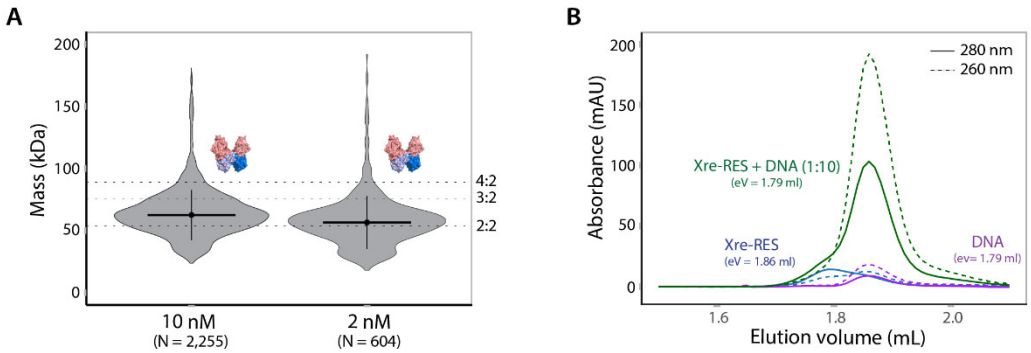

372
373 **Figure 6. Isolation of a non-binding 2:2 Xre-RES^{Pp} complex**. **A.** Single-molecule mass determination of
374 Xre$_{His6}$-RES^{Pp} on the 2:2 complex form at 10 nM (left) or 2 nM (right). Violin plots show the density of all
375 events (N). Solid black horizontal line indicates the median mass, while the vertical line shows the standard
376 deviation (SD). Theoretical masses of the Xre-RES$^{Pp}_{His6}$ complex with 4:2, 3:2, and 2:2 stoichiometries are
377 indicated by dotted lines. **B.** High resolution analytical SEC (a-SEC) analysis of Xre$_{NHis6}$-RES (Xre-RES,
378 blue), S4 (DNA, purple), or DNA mixed with protein in a 1:10 ratio (Xre-RES + DNA, green). Elution
379 volumes are noted. Full line shows 280 nm absorbance, while dotted line is 260 nm absorbance.

380

381 **DISCUSSION**

382 In this study, we present a detailed analysis of the transcriptional regulation of the Cro-like type II
383 TA system Xre-RES^{Pp}. We show that the intact, heterohexameric TA complex efficiently represses
384 transcription from the *xre-res* locus through direct binding to an imperfect inverted repeat region
385 overlapping with the σ^{70} element in the promoter region. We confirm that the unusual 4:2
386 stoichiometry of the TA complex observed in the crystal structure (11), in which each of the toxins
387 of a central dimer interacts with a dimer of antitoxins, is present in solution, while isolated Xre^{Pp}
388 antitoxin is a monomer and only weakly represses transcription *in vivo*. This suggests that the
389 formation of the Xre dimer is necessary for efficient binding to DNA and that the Xre dimer is
390 stabilised through interaction with the RES dimer. Supportive of this, we identified a 2:2 complex
391 present at low complex concentration, which does not bind DNA. Together, these data allow us to
392 propose a model for transcriptional regulation in which a low cellular concentration of the Xre
393 antitoxin leads to dissociation of the RES-bound Xre dimer and thereby the formation of a 2:2
394 complex (**Figure 7**). In this 2:2 complex, Xre still binds to, and thus neutralises, the RES toxin but
395 it cannot bind DNA and consequently, the RNAP holoenzyme binds the promoter and the *xre-res*^{Pp}
396 operon is expressed. When the concentration of the Xre antitoxin increases, a DNA-binding 4:2
397 complex is formed, presumably via the 3:2 intermediate identified by single-molecule mass
398 determination (**Figure 5E**), and expression of *xre-res*^{Pp} is repressed.

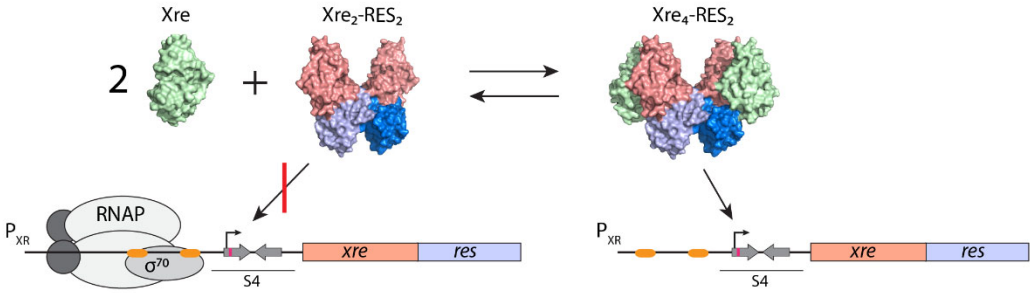

399
400 **Figure 7. Model for transcriptional regulation of the *xre-res*^{Pp} operon**. At low concentrations of Xre
401 antitoxin, two Xre monomers dissociate from the Xre-RES^{Pp} complex and a neutralising, non-binding 2:2

402 complex is formed (Xre_2-RES_2). In this situation, RNA polymerase (RNAP) bound to the σ^{70} subunit can
403 bind the -35 and -10 elements (orange ovals) of the P_{XR} promoter and initiate transcription. When the
404 concentration of Xre increases, a 4:2 complex is formed (Xre_4-RES_2), which binds the imperfect inverted
405 repeat (S4, grey arrows with mismatch marked in red), repressing transcription of the *xre-res*^{Pp} operon.
406

407 The proposed model of transcriptional regulation deviates from classical conditional cooperativity,
408 in which a complex with a 1:1 toxin:antitoxin ratio would have a strong DNA binding affinity,
409 while increasing the toxin:antitoxin above that would decrease the DNA binding affinity (22). Our
410 model more resembles the recently proposed translation-responsive model (27). In this model, the
411 relative concentration of antitoxin is also paramount but regulated by differential translation, while
412 proteolytic degradation of the antitoxin is a constant. Moreover, transcriptional repression of the TA
413 operon by the TA complex is a dynamic equilibrium between a non-binding, toxin-neutralising
414 complex, formed when the concentrations between antitoxin and toxin are similar, and a repressive
415 complex only formed at high antitoxin concentrations. A dynamic equilibrium between a 2:2 and a
416 4:2 TA complex was also recently observed for the ParDE1 TA system from *M. tuberculosis* (28).
417 In general, ParE toxins share a conserved protein fold with the RelE/ParD superfamily and targets
418 DNA gyrase (29, 30), and a model for ParE1 toxin release was proposed in which two 2:2 ParDE1
419 complexes remodel into a 4:2 complex and free, active ParE1 toxin. This is different from the Xre-
420 RES^{Pp} system, in which it is the addition of Xre monomers that leads to the formation of a 4:2
421 complex. We have not observed free RES toxin in any of our purifications and our data indicate that
422 the toxin-bound Xre monomer is strongly associated.
423

424 As the *xre-res* operon is present in many bacterial genomes (10), we wondered to which extent the
425 proposed model is unique for the *P. putida* locus or applies more generally. For the Xre-RES system
426 from *M. tuberculosis*, MbcAT, the crystal structure revealed a donut-like heterododecamer
427 consisting of three heterotetramers with the antitoxins (MbcA) pointing inwards. This higher-order
428 structure thus questions the ability of this complex to access and bind DNA (12). For the *S. meliloti*

429 system, ParST, the crystal structure was determined of a trypsin-digested TA complex with the
430 DNA-binding domains missing (13). Yet, the recently published crystal structure of VPA0770-
431 VPA0769 from *V. parahaemolyticus* is similar to Xre-RES^{Pp} and moreover, this system was also
432 found to exist in an equilibrium between an antitoxin dimer and a monomer (17). It is thus possible
433 that the model could apply to at least some of the other Xre-RES like TA systems.
434
435 We show that the 4:2 Xre-RES^{Pp} complex binds strongly to an imperfect inverted repeat (S4) in the
436 promoter region and that the asymmetry of imperfect inverted repeat appears to be important for
437 optimal protein-DNA interaction. In addition, the HTH DNA-binding domains in 4:2 complex are
438 also by nature asymmetrical, suggesting that they could control directionality of the Xre-RES^{Pp}
439 protein complex upon binding to DNA. Despite the presence of two complete dsDNA binding sites
440 in the Xre-RES^{Pp} complex, we were only capable of showing binding to a single copy of S4
441 dsDNA. It is thus possible that directional binding of Xre-RES^{Pp} to S4 only involves one Xre^{Pp}
442 dimer and positions the second dimer to bind another operator site, possibly located in the S1-S2
443 region of the promoter as removal of this led to increased promoter activity. The intactness of the
444 imperfect inverted repeat was also found to be important for promoter activity, as changes affecting
445 the TSS (+1) completely disrupted transcription. The identity of the initiating nucleoside
446 triphosphate (iNTP) has previously been shown to be pivotal for promoters of genes that are up-
447 /downregulated during the stringent response in *Bacillus subtilis* (31). It is thus possible that the
448 lack of transcription observed for the P_{XR}ΔS4 and P_{XR}5'-flip variants is caused by a change in the
449 identity of the iNTP (T to A for P_{XR}ΔS4, and T to C for P_{XR}5'-flip).
450
451 In conclusion, transcriptional regulation of the *xre-res*^{Pp} operon appears to rely on the imperfectness
452 of the operator site, allowing both efficient transcription by RNAP and repression by the Xre-RES^{Pp}

453 complex, as well on a dynamic and concentration-dependent stoichiometry of the Xre-RES^{Pp}
454 complex. Together, these features ensure that transcription occurs in that exact moment that Xre-
455 RES^{Pp} is released from the DNA, leading to expression of *xre-res*^{Pp} and thus an increase in the
456 concentration of Xre and renewed transcriptional repression.
457

458 **MATERIALS AND METHODS**

459 **Bacterial strains and plasmids**

460 Bacterial strains and plasmids used in this study are listed in **Table S1**, and DNA oligonucleotides
461 in **Table S2**. Detailed descriptions of plasmid construction are found in **Supplementary Methods**.
462 For site-directed mutagenesis, the Q5 Site-Directed Mutagenesis Kit from NEB was used according
463 to the protocol and mutagenesis primers were designed using NEBaseChanger.
464

465 **Measurements of promoter activities and *in vivo* repression**

466 For promoter activity assays, *E. coli* MG1655 was co-transformed with transcriptional fusion vector
467 pGH254Kgfp and a pBAD33 vector. Overnight cultures were grown in M9 medium supplemented
468 with 0.2% Casamino acids, 0.4% glycerol, 50 mg/ml chloramphenicol, 25mg/ml kanamycin and
469 0.2% glucose. Overnight cultures were washed once in M9 medium and diluted to 0.03 in M9
470 medium supplemented with 0.2% Casamino acids, 0.4% glycerol, 50 µg/ml chloramphenicol and
471 25µg/ml kanamycin. From this, cultures were split into non-induced or induced (by 0.2% arabinose)
472 sub-cultures. Samples of 200 µl were grown in triplicates in a black/clear bottom 96-well plates
473 (Thermo Scientific^{TM}, cat. no. 165305), using a Synergy H1 microplate reader (BioTek). Optical
474 density (600 nm) and fluorescence intensity (excitation, 479 nm; emission, 520 nm) was measured
475 every 5 min for 12 h. A strain with empty pGH254Kgfp and pBAD33 was used as control and
476 fluorescence intensity at a specific time point was calculated as described by (32), using the formula

477 $I(t) = I_u(t) - \frac{A(t)}{B(t)} I_b(t)$ where $I(t)$ is the fluorescence intensity at a specific time point, $I_u(t)$ is the
478 uncorrected intensity, $A(t)/B(t)$ is the absorbance ration between the measured culture and the
479 culture used as blank, and $I_b(t)$ is the fluorescence intensity of the culture used as blank. The
480 calculated fluorescent intensity was divided by OD_{600} to obtain corrected fluorescence intensity per
481 OD_{600} unit relative to the control strain (relative fluorescence units, RFU). The assay was repeated
482 three times for each strain. Mean values were calculated for technical triplicates and used to
483 calculate a mean-of-mean values and standard mean of error (SEM) of biological triplicates.
484 Statistical analysis was performed in Prism (GraphPad Software Inc.) using two-way analysis of
485 variance (ANOVA) followed by Dunnett's multiple comparisons test to determine significant
486 differences. Statistical significance was defined as $p < 0.05$. Graphs and statistical analyses were
487 prepared with Prism.
488
489 **Protein expression and purification**
490 For protein expression, plasmids pETDuet::*res*$_{NHis6}$-*xre*^{Pp}, pETDuet::*xre*$_{NHis6}$-*res*^{Pp}, or pET-
491 29b(+)::*xre*$_{CHis6}^{Pp}$ were transformed into *E. coli* BL21(DE3). Cells were grown to an OD_{600} of 0.6-
492 0.8, induced by the addition of 0.5 mM IPTG for 20-22 h at 20°C, and harvested by centrifugation
493 (6,000 rpm, 20 min, 4°C).
494
495 For purification of the Xre-RES$^{Pp}_{NHis6}$ and the Xre$_{NHis6}$-RES^{Pp} complex, cell pellets were
496 resuspended in lysis buffer (50 mM Tris-HCl, pH 8.5, 300 mM KCl, 10 mM imidazole)
497 supplemented with 1 ng/µl DNase I and 1 mM phenylmethylsulfonyl fluoride (PMSF). Cells were
498 lysed by high-pressure homogenization (Avestin) at 15,000 psi, and clarified by centrifugation
499 (14,000 rpm, 45 min, 4°C). Clarified cell lysates were loaded onto a 1 ml HisTrap FF column
500 (Cytiva) and columns were washed with lysis buffer including 30 mM imidazole. Protein

501 complexes were eluted with elution buffer (50 mM Tris-HCl, pH 8.5, 150 mM KCl, 300 mM
502 imidazole) and further purified using a 1 ml Source 15Q column (GE Healthcare), running in buffer
503 A (50 mM Tris-HCl, pH 8.5, 5 mM β-mercaptoethanol (BME) and a gradient into buffer B (50 mM
504 Tris-HCl, pH 8.5, 5 mM BME, 1 M KCl). Final separation was achieved on a Superdex 200
505 Increase 10/300 GL column (GE Healthcare) equilibrated in gel filtration buffer (20 mM HEPES-
506 KOH, pH 7.5, 150 mM KCl, 5 mM $MgCl_2$, 3 mM BME) (**Figure S5**).
507
508 For purification of Xre alone (Xre_{CHis6}^{Pp}), cell pellets were resuspended in lysis buffer (50 mM
509 HEPES-KOH, pH 7.5, 400 mM KCl, 10 mM imidazole) supplemented with 1 ng/µl DNase I and 1
510 mM PMSF, lysed by high-pressure homogenization (Avestin) at 15,000 psi, and clarified by
511 centrifugation (14,000 rpm, 45 min, 4°C). Clarified cell lysate was loaded onto a 1 ml HisTrap FF
512 column (Cytiva), washed with lysis buffer including 30 mM imidazole and eluted using 300 mM
513 imidazole. Eluate was precipitated overnight at room temperature with 45% ammonium sulphate
514 (AmS) and clarified by centrifugation (20.000 rpm, 30 min, 20° C). Supernatant was collected and
515 further precipitated with 60% AmS overnight. Precipitated protein was collected by centrifugation
516 (20.000 rpm, 30 min, 20° C) and resuspended in gel filtration buffer (20 mM HEPES-KOH, pH 7.5,
517 150 mM KCl, 3 mM BME) until conductivity was 15 mS/cm. Final separation was achieved on a
518 Superdex 75 10/300 GL column (GE Healthcare) equilibrated in gel filtration buffer (**Figure S5**).
519
520 **Analytical Size Exclusion Chromatography**
521 To screen the interaction between the Xre-RES^{Pp} complex and putative binding sites within the
522 promoter, 30 bp dsDNA oligos corresponding to S1, S2, S3 or S4 in the promoter region (**Figure**
523 **1A**) were made using oligos specified in **Table S2**,. Briefly, equimolar amounts of complementary
524 DNA oligos were mixed in milliQ water heated to 95°C and cooling to room temperature.

525 Concentrations were determined by nanodrop, using calculated extinction coefficients, and 1.5
526 nmoles of dsDNA and/or purified Xre-RES$^{Pp}_{His6}$ each were incubated for 5 min at 37° C. Samples
527 containing protein alone, DNA alone, or mixed protein and DNA were analysed by analytical gel
528 filtration (a-SEC) using a Superdex 200 Increase 10/300 GL column (GE Healthcare) running in
529 DNA binding buffer (20 mM HEPES pH 7.5, 150 mM KCl, 5 mM $MgCl_2$ and 3 mM BME). To
530 assess stoichiometry of protein to DNA in the interaction, samples with protein to DNA ratios of
531 2:1, 1:2, and 1:10 were analyzed by a-SEC and SEC-Multi angle light scattering (MALS) in DNA
532 binding buffer. For 1:2 and 1:10 ratios of protein to DNA, a Superdex 200 Increase 3.2/300 GL
533 column (GE Healthcare) was used for increased resolution. Data was plotted in R (version 4.3.1)
534 using the Tidyverse package (33).
535
536 **SEC-MALS**
537 For ensemble mass determination, purified protein complex was applied to a size-exclusion column
538 (SEC) coupled to multi angle light scattering (MALS) in DNA binding buffer (20 mM HEPES pH
539 7.5, 150 mM KCl, 5 mM $MgCl_2$, 3 mM BME). For each sample, 20-40 µg was added to a Superose
540 6 increase 10/300 column (GE Healthcare) and MALS spectra was recoded using inline DAWN-
541 HELEOS light scattering and optilab T-rEX refractive index detectors (Wyatt). Mass was
542 determined by analyzing the differential refractive index using the Debye model for proteins (34)
543 integrated in the ASTRA VI software. Data was plotted in R (version 4.3.1) using the Tidyverse
544 package (33).
545
546 **Mass photometry**
547 Single molecule mass determination was carried out using the TwoMP mass photometer (Refeyn).
548 Experimental data was acquired through one-minute videos recorded by AcquireMP (ver 2.5)

549 software on precleaned high-precision coverslips with Culterwell^{TM} gaskets (Grace Biolabs). Focus
550 was automatically found by AcquireMP and was deemed correct when the variance was 0.01. Prior
551 to protein analysis, a mass calibration was performed using Bovine Serum Albumin (BSA) and
552 either Immunoglobulin M (IgM) or α2 macroglobulin (α2M) spanning a mass range of 66 kDa to
553 720 kDa. Standard samples were collected at final concentrations of 10 nM by 10-fold dilution into
554 gel filtration buffer. Collected videos were analyzed in DiscoverMP (ver 2.5) by fitting Gaussian
555 functions to ratiometric contrast values of all events in the video. Mass determination was done by
556 fitting a linear curve between ratiometric contrast and molar mass of standard proteins. The Xre^{Pp}-
557 RES^{Pp} complex was diluted 10-fold, 20-fold, or 40-fold in gel filtration buffer (20 mM HEPES pH
558 7.5, 150 mM KCl, 5 mM $MgCl_2$, 3 mM BME) to achieve final concentrations of 10, 5, and 2 nM,
559 respectively. Videos were collected as with the standards and mass was determined from the
560 calibration curve. Statistical significance was defined using a Bonferroni corrected p value of
561 0.0055, to avoid the multiple comparisons problem. Normality was tested using the Kolmogorov-
562 Smirnov test, and populations were compared using the Wilcoxon test.
563

564 **Isothermic titration calorimetry**

565 Thermodynamic constant determination was carried out using the PEAQ-ITC (Malvern
566 panalytical). Purified protein and dsDNA samples were dialyzed into the DNA binding buffer (20
567 mM HEPES pH 7.5, 150 mM KCl, 5 mM $MgCl_2$, 3 mM BME), after which 20 μM of Xre-
568 RES$^{Pp}_{Nhis6}$ was added to the sample chamber and 300-700 μM dsDNA was titrated in through 13 to
569 17 injections. Each dataset was baseline-corrected by independent measurements of buffer into
570 buffer, titrant into buffer, and buffer into sample. Data analysis was done using Microcal PEAQ-
571 ITC Analysis Software (Malvern panalytical). Data quality was evaluated through minimizing

572 residuals, as well as approximating active concentrations of protein and titrant for fitting to correct
573 N. Reported values are a mean of three independent replicates.
574

575 **ACKNOWLEDGEMENTS**

576 This work was supported by grants from the Independent Research Fund Denmark (grant 0135-
577 00072B) and the Novo Nordisk Foundation (grants NNF18OC0030646 and NNF22OC0079855) to
578 D. E. B. The authors would like to thank Janni Nielsen and Prof. Daniel E. Otzen for help with
579 SEC-MALS, Lan Bich Van for technical assistance with protein purification, and Dr. Kristoffer
580 Winther for help with identification of the four promoter repeat sequences. We also wish to thank
581 Associate professor Magnus Kjærgaard and the MBG Biophysics Core Facility for use of
582 equipment supported by The Carlsberg Foundation.
583

584 **REFERENCES**

585 1. Browning DF, Busby SJW. 2004. The regulation of bacterial transcription initiation. Nat Rev
586 Microbiol 2:57–65.
587 2. Busby S, Ebright RH. 1994. Promoter structure, promoter recognition, and transcription
588 activation in prokaryotes. Cell 79:743–746.
589 3. Burgess RR, Travers AA, Dunn JJ, Bautz EKF. 1969. Factor stimulating transcription by
590 RNA polymerase. Nature 221:43–46.
591 4. Ishihama A. 2000. Functional modulation of Escherichia coli RNA polymerase. Annu Rev
592 Microbiol 54:499–518.
593 5. Jacob F, Monod J. 1961. Genetic regulatory mechanisms in the synthesis of proteins. J Mol
594 Biol 3:318–56.
595 6. Aravind L, Anantharaman V, Balaji S, Babu MM, Iyer LM. 2005. The many faces of the
596 helix-turn-helix domain: Transcription regulation and beyond. FEMS Microbiol Rev 29:231–
597 262.
598 7. Slattery M, Zhou T, Yang L, Dantas Machado AC, Gordân R, Rohs R. 2014. Absence of a
599 simple code: how transcription factors read the genome. Trends Biochem Sci 39:381–99.
600 8. Fernandez-Lopez R, Ruiz R, del Campo I, Gonzalez-Montes L, Roeland Boer D, de la Cruz
601 F, Moncalian G. 2022. Structural basis of direct and inverted DNA sequence repeat
602 recognition by helix–turn–helix transcription factors. Nucleic Acids Res 50:11938–11947.
603 9. John J, Jabbar J, Badjatia N, Rossi MJ, Lai WKM, Pugh BF. 2022. Genome-wide promoter
604 assembly in E. coli measured at single-base resolution. Genome Res 32:878–892.
605 10. Makarova KS, Wolf YI, Koonin E V. 2009. Comprehensive comparative-genomic analysis
606 of type 2 toxin-antitoxin systems and related mobile stress response systems in prokaryotes.

607 Biol Direct 4:19.
608 11. Skjerning RB, Senissar M, Winther KS, Gerdes K, Brodersen DE. 2018. The RES domain
609 toxins of RES-Xre toxin-antitoxin modules induce cell stasis by degrading NAD. Mol
610 Microbiol 0:1–16.
611 12. Freire DM, Gutierrez C, Garza-Garcia A, Grabowska AD, Sala AJ, Ariyachaokun K,
612 Panikova T, Beckham KSH, Colom A, Pogenberg V, Cianci M, Tuukkanen A, Boudehen
613 YM, Peixoto A, Botella L, Svergun DI, Schnappinger D, Schneider TR, Genevaux P, de
614 Carvalho LPS, Wilmanns M, Parret AHA, Neyrolles O. 2019. An NAD + Phosphorylase
615 Toxin Triggers Mycobacterium tuberculosis Cell Death. Mol Cell 73:1282-1291.e8.
616 13. Piscotta FJ, Jeffrey PD, James Link A. 2019. ParST is a widespread toxin–antitoxin module
617 that targets nucleotide metabolism. Proc Natl Acad Sci U S A 116:826–834.
618 14. Harms A, Brodersen DE, Mitarai N, Gerdes K. 2018. Toxins, Targets, and Triggers: An
619 Overview of Toxin-Antitoxin Biology. Mol Cell 1–17.
620 15. Kusumawardhani H, van Dijk D, Hosseini R, de Winde JH. 2020. Novel Toxin-Antitoxin
621 Module SlvT-SlvA Regulates Megaplasmid Stability and Incites Solvent Tolerance in
622 Pseudomonas putida S12. Appl Environ Microbiol 86:1–17.
623 16. Zhou J, Li S, Li H, Jin Y, Bai F, Cheng Z, Wu W. 2021. Identification of a toxin–antitoxin
624 system that contributes to persister formation by reducing nad in pseudomonas aeruginosa.
625 Microorganisms 9.
626 17. Zhang Y, Song X, Chen C, Liu L, Xu Y, Zhang N, Huang W, Zheng J, Yuan W, Tang L, Lin
627 Z. 2023. Structural insights of the toxin-antitoxin system VPA0770-VPA0769 in Vibrio
628 parahaemolyticus. Int J Biol Macromol 242:124755.
629 18. Brennan RG, Matthews BW. 1989. The helix-turn-helix DNA binding motif. J Biol Chem
630 264:1903–1906.
631 19. Fraikin N, Goormaghtigh F, Van Melderen L. 2020. Type II Toxin-Antitoxin Systems:
632 Evolution and Revolutions. J Bacteriol 202:1–14.
633 20. Garcia-Pino A, Balasubramanian S, Wyns L, Gazit E, De Greve H, Magnuson RD, Charlier
634 D, van Nuland NAJ, Loris R. 2010. Allostery and intrinsic disorder mediate transcription
635 regulation by conditional cooperativity. Cell 142:101–11.
636 21. Overgaard M, Borch J, Jørgensen MG, Gerdes K. 2008. Messenger RNA interferase RelE
637 controls relBE transcription by conditional cooperativity. Mol Microbiol 69:841–57.
638 22. Boggild A, Sofos N, Andersen KR, Feddersen A, Easter AD, Passmore LA, Brodersen DE.
639 2012. The crystal structure of the intact E. coli RelBE toxin-antitoxin complex provides the
640 structural basis for conditional cooperativity. Structure 20:1641–1648.
641 23. Bruyn P De, Girardin Y, Loris R. 2021. Prokaryote toxin–antitoxin modules: Complex
642 regulation of an unclear function. Protein Sci 1103–1113.
643 24. Cormack BP, Valdivia RH, Falkow S. 1996. FACS-optimized mutants of the green
644 fluorescent protein (GFP). Gene 173:33–38.
645 25. Takeda Y, Folkmanis A, Echols H. 1977. Cro Regulatory by Bacteriophage. J Biol Chem
646 252:6177–6183.
647 26. Shimon LJW, Harrison SC. 1993. The phage 434 OR2/R1-69 complex at 2.5 Å resolution. J
648 Mol Biol https://doi.org/10.1006/jmbi.1993.1434.
649 27. Ramisetty BCM. 2020. Regulation of Type II Toxin-Antitoxin Systems: The Translation-
650 Responsive Model. Front Microbiol 11:1–6.
651 28. Beck IN, Arrowsmith TJ, Grobbelaar MJ, Mar J, Blo TR, Bromley EHC. 2023. Toxin release
652 by conditional remodelling of ParDE1 from Mycobacterium tuberculosis leads to gyrase
653 inhibition. Nucleic Acids Res 1–21.
654 29. Jiang Y, Pogliano J, Helinski DR, Konieczny I. 2002. ParE toxin encoded by the broad-host-

range plasmid RK2 is an inhibitor of Escherichia coli gyrase. Mol Microbiol 44:971–979.
30. Dalton KM, Crosson S. 2010. A conserved mode of protein recognition and binding in a ParD-ParE toxin - antitoxin complex. Biochemistry 49:2205–2215.
31. Krásný L, Tišerová H, Jonák J, Rejman D, Šanderová H. 2008. The identity of the transcription +1 position is crucial for changes in gene expression in response to amino acid starvation in Bacillus subtilis. Mol Microbiol 69:42–54.
32. Jurenas D, Fraikin N, Goormaghtigh F, De Bruyn P, Vandervelde A, Zedek S, Jové T, Charlier D, Loris R, Van Melderen L. 2021. Bistable Expression of a Toxin-Antitoxin System Located in a Cryptic Prophage of Escherichia coli O157:H7. MBio 12:1–15.
33. Wickham H, Averick M, Bryan J, Chang W, McGowan L, François R, Grolemund G, Hayes A, Henry L, Hester J, Kuhn M, Pedersen T, Miller E, Bache S, Müller K, Ooms J, Robinson D, Seidel D, Spinu V, Takahashi K, Vaughan D, Wilke C, Woo K, Yutani H. 2019. Welcome to the Tidyverse. J Open Source Softw 4:1686.
34. Edelman J. 1992. The low-temperature heat capacity of solid proteins. Biopolymers 32:209–18.

SUPPLEMENTARY METHODS

Plasmid constructions

For pBAD33::*xre*$_{opSD}$, *P. putida* KT2440 *xre* (PP_RS12675) was amplified from pUC57::*xre-res*^{Pp} using primer xre_opSD_Fw, adding an optimized SD (opSD) to the 3'-end, and primer xre_Rv. The resulting PCR product was digested with KpnI and SalI and ligated into pBAD33.

For pBAD33::*xre*$_{naSD}$-*res*^{Pp}, *P. putida* KT2440 *xre-res* locus (PP_RS12675- PP_RS12680) was amplified from pUC57::*xre-res*^{Pp} using primer xre_naSD_Fw, including the native SD (opSD) at the 3'-end, and primer res_Rv. The resulting PCR product was digested with KpnI and SalI and ligated into pBAD33.

For pGH254Kgfp, the *lacZYA* operon from pGH254K was replaced with *gfpmut2* using Gibson Assembly (NEB) according to the protocol. The *gfpmut2* gene encodes a GFP mutant containing a triple substitution; S65A, V68L, and S72A, that confers enhanced fluorescence emission and more efficient folding at 37°C (Cormack et al., 1996). The vector backbone was amplified from pGH254K using primer pGH254K_gib_Fw and pGH254K_gib_Rv, while the *gfpmut2* insert was amplified from synthetic DNA ordered from Twist Bioscience. Sequencing revealed an insertion (T6613) in the ribosomal binding site (RBS), which was removed using the Q5 Site-Directed Mutagenesis Kit from NEB. Primers pGH254Kgfp_T6613_Fw and pGH254Kgfp_T6613_Rv were designed using NEBaseChanger.

For pGH254Kgfp::P_{XR}, The *xre-res* promoter (P_{XR}) was amplified from pUC57::*xre-res* using primers PXR_Fw and PXR_Rv. The resulting PCR product was digested with EcoRI and BamHI and ligated into pGH254Kgfp.

For pGH254Kgfp::P_{XR}ΔS1, deletion of S1 from P_{XR}, corresponding to basepair 1-34, was done using Q5 Site-Directed Mutagenesis Kit from NEB with pGH254Kgfp::P_{XR} as the template and primers PXRΔS1_Fw and PXRΔS1_Rv.

For pGH254Kgfp::P_{XR}ΔS1-2, deletion of S1-2 from P_{XR}, corresponding to basepair 1-71, was done using Q5 Site-Directed Mutagenesis Kit from NEB with pGH254Kgfp::P_{XR} as the template and primers PXRΔS1-2_Fw and PXRΔS1-2_Rv.

For pGH254Kgfp::P_{XR}ΔS1-3, deletion of S1-3 from P_{XR}, corresponding to basepair 1-101, was done using Q5 Site-Directed Mutagenesis Kit from NEB with pGH254Kgfp::P_{XR} as the template and primers PXRΔS1-3_Fw and PXRΔS1-3_Rv.

For pGH254Kgfp::P_{XR}ΔS4, deletion of S4 from P_{XR}, corresponding to basepair 107-137, was done using Q5 Site-Directed Mutagenesis Kit from NEB with pGH254Kgfp::P_{XR} as the template and primers PXRΔS4_Fw and PXRΔS4_Rv.

For pGH254Kgfp::P_{XR}ΔS3-4, deletion of S3-4 from P_{XR}, corresponding to basepair 71-137, was done using Q5 Site-Directed Mutagenesis Kit from NEB with pGH254Kgfp::P_{XR} as the template and primers PXRΔS3-4_Fw and PXRΔS3-4_Rv.

For pGH254Kgfp::P_{XR}Δrepeat, deletion of sequence 3-4 from P_{XR}, corresponding to basepair 115-129, was done using Q5 Site-Directed Mutagenesis Kit from NEB with pGH254Kgfp::P_{XR} as the template and primers PXRΔrepeat_Fw and PXRΔrepeat_Rv.

For pGH254Kgfp::P_{XR}-5'perfect, substitution G115T in P_{XR}, generating a perfect 5'-repeat in Sequence 4, was done using Q5 Site-Directed Mutagenesis Kit from NEB with pGH254Kgfp::P_{XR} as the template and primers PXR-5'perf_Fw and PXR-5'perf_Rv.

For GH254Kgfp::P_{XR}-3'perfect, substitution A130C in P_{XR}, generating a perfect 3'-repeat in Sequence 4, was done using Q5 Site-Directed Mutagenesis Kit from NEB with pGH254Kgfp::P_{XR} as the template and primers PXR-3'perf_Fw and PXR-3'perf_Rv.

For pGH254Kgfp::P_{XR}-5'flip, substitution 113-TTGTCG-118 to CGACAA in P_{XR}, destroying 5'-repeat in Sequence 4, was done using Q5 Site-Directed Mutagenesis Kit from NEB with pGH254Kgfp::P_{XR} as the template and primers PXR-5'flip_Fw and PXR-5'flip_Rv.

For pGH254Kgfp::P_{XR}-3'flip, substitution 129-CGAAAA-134 to TTTTCG in P_{XR}, destroying 3'-repeat in Sequence 4, was done using Q5 Site-Directed Mutagenesis Kit from NEB with pGH254Kgfp::P_{XR} as the template and primers PXR-3'flip_Fw and PXR-3'flip_Rv.

For pET-29b(+)::xre_{CHis6}^{Pp}, *P. putida* KT2440 *xre* (PP_RS12675) was designed to fuse a C-terminal His_6-tag directly onto the C-terminal of Xre, followed by a stop codon (xre_{CHis6}). The construct was custom synthesized by Twist Bioscience and cloned into pET-29b(+) using restriction sites NdeI and XhoI.

For pETDuet::*res*$_{NHis6}$-*xre*^{Pp}, *P. putida* KT2440 *xre* (PP_RS12675) was amplified from pUC57::*xre-res*^{Pp} using primer xre_mcsII_Fw and xre_mcsII_Rv. The resulting PCR product was digested with NdeI and XhoI and ligated into MCSII of pETDuet-1 to generate pETDuet::*xre(mcsII)*. Subsequently, *P. putida* KT2440 *res* (PP_RS12680) and was amplified from pUC57::*xre-res*^{Pp} using primer res_mcsI_Fw and res_mcsI_Rv. The resulting PCR product was digested with BamHI and SalI and ligated into MCSI of pETDuet::*xre(mcsII)*.

For pETDuet::*xre*$_{NHis6}$-*res*^{Pp}, *P. putida* KT2440 *xre* (PP_RS12675) and was amplified from pUC57::*xre-res*^{Pp} using primer xre_mcsI_Fw and xre_mcsI_Rv. The resulting PCR product was digested with BamHI and SalI and ligated into MCSI of pETDuet-1 to generate pETDuet::*xre(mcsI)*. Subsequently, *P. putida* KT2440 *res* (PP_RS12680) was amplified from pUC57::*xre-res*^{Pp} using primer res_mcsI_Fw and res_mcsI_Rv. The resulting PCR product was digested with NdeI and XhoI and ligated into MCSII of pETDuet::*xre(mcsI)*.

References

Cormack, B. P., Valdivia, R. H., & Falkow, S. (1996). FACS-optimized mutants of the green fluorescent protein (GFP). *Gene*, *173*(1), 33–38. https://doi.org/10.1016/0378-1119(95)00685-0

Asymmetry of both repressor and operator is important for the transcriptional regulation of the *P. putida* Xre-RES system

Frederik Oskar G. Henriksen, Ditlev E. Brodersen, and Ragnhild B. Skjerning[*]

SUPPLEMENTARY FIGURES

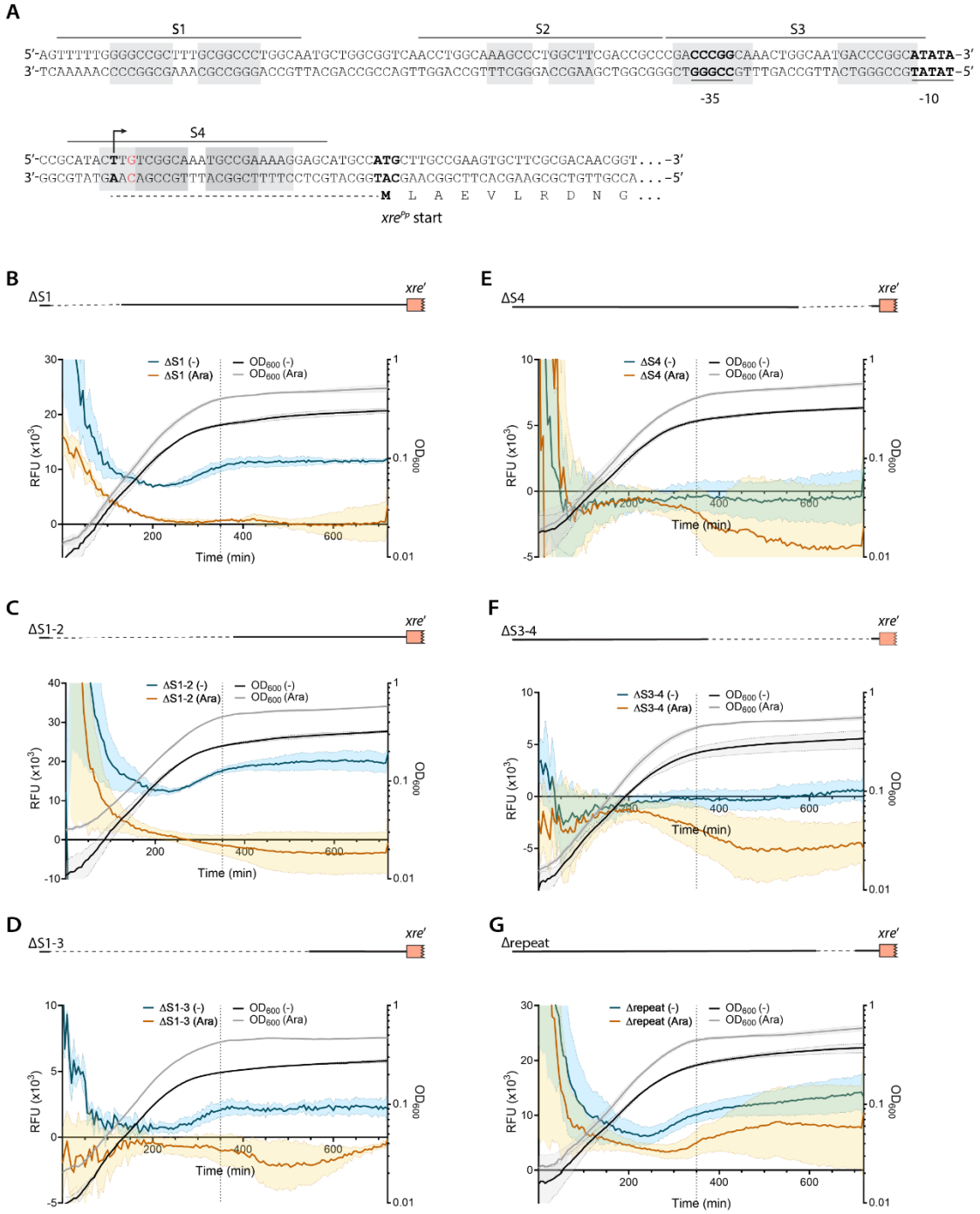

Figure S1. Determination of the minimal promoter requirements of P_{XR}. A. Native DNA sequence of the P_{XR} promoter. The S1 (inverted repeat), S2 (inverted repeat), S3 repeat (directional repeat), and S4 (imperfect inverted repeat) sequences are indicated with lines and light grey boxes marking the repeat. The perfect part of the S4 repeat is shown with a dark grey box and the mismatch in the first repeat is in red. The location of the σ^{70}-35 and -10 promoter elements and the transcription start site (TSS, arrow) are indicated. The *xre*^{Pp} start codon is marked with bold letters, and N-terminal residues noted below. **B-G**. Promoter activity measured as GFP relative fluorescence units (RFU) during growth without (-) or with arabinose (Ara) for *E. coli* MG1655 containing the promoter reporter plasmid pGH254Kgfp with the indicated promoter variations, as well as the pBAD33::*xre*$_{naSD}$-*res*^{Pp} vector (*xre-res*). The curves show mean-of-mean values (line) with SEM (shadow). The dotted line indicates the 350 min time point used in **Figure 2B**. A schematic representation of the construct is included above each graph.

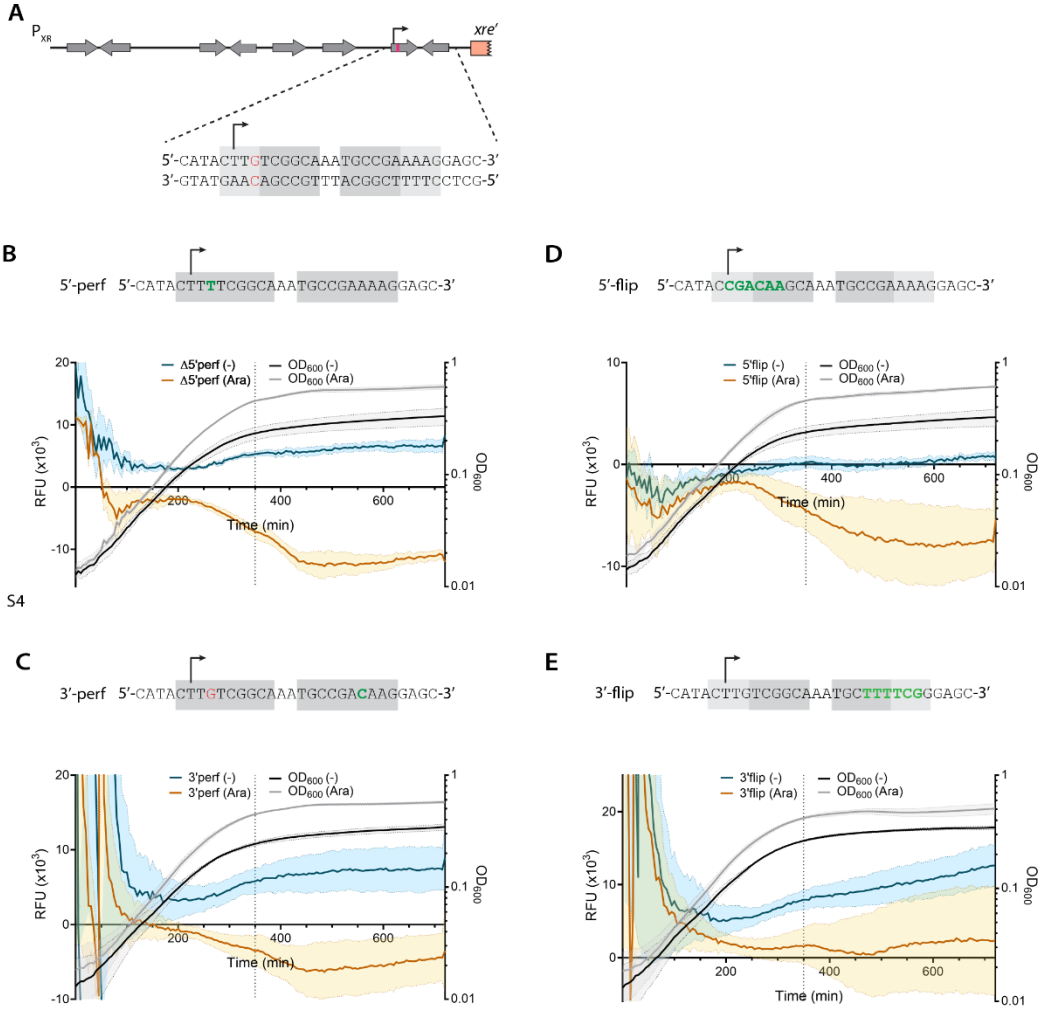

Figure S2. Functional analysis of the S4 repeat sequence. **A.** Schematic representation of the P_{XR} promoter, including 30 bp of the 5' region of the *xre*^{Pp} (*xre*') gene. The TSS is indicated by a bent arrow. The DNA sequence of the imperfect inverted repeat is highlighted (light grey), including the mismatch in the first repeat (red) and the perfect part (dark grey). **B-E**. Promoter activity measured as GFP relative fluorescence units (RFU) during growth without (-) or with arabinose (Ara) for *E. coli* MG1655 containing the promoter reporter plasmid pGH254Kgfp with the indicated promoter variations, as well as the pBAD33::*xre*$_{naSD}$-*res*^{Pp} vector (*xre-res*). The curves show mean-of-mean values (line) with SEM (shadow). The dotted line indicates the 350 min time point used in **Figure 3B**. A schematic representation of the construct is included above each graph with DNA modifications shown in green.

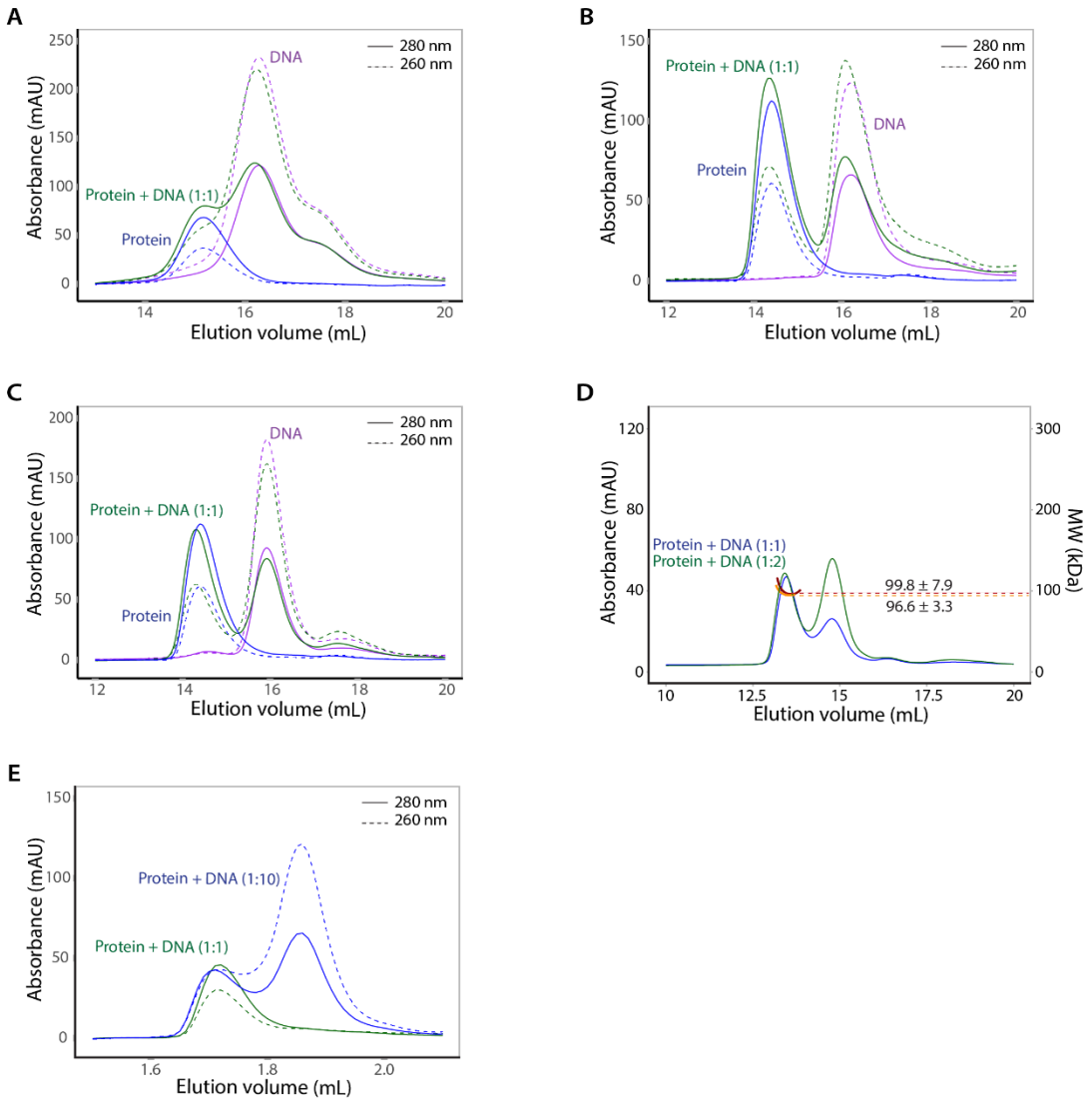

Figure S3. Xre-RES^{Pp} interacts specifically with S4 in a 1:1 protein complex to DNA duplex ratio. **A-C**. Analytical SEC (a-SEC) analysis of Xre-RES$^{Pp}_{His6}$ binding to S1 (**A**), S2 (**B**), or S3 (**C**). Chromatograms show elution profiles for Xre-RES$^{Pp}_{His6}$ (Protein, blue), DNA (purple), or DNA mixed with protein in a 1:1 ratio (Protein + DNA 1:1, green). Full lines show 280 nm and dotted lines 260 nm absorbance. **D**. SEC-MALS analysis of the change in mass of Xre-RES$^{Pp}_{His6}$ mixed with DNA (S4). Chromatogram shows elution profiles for 1:1 (blue) or 1:2 (green) protein complex to DNA duplex ratios, as well as mass of peak for 1:1 (yellow) and 1:2 (red). Masses were determined to 96.6 ± 3.3 (1:1 ratio) and 99.8 ± 7.9 kDa (1:2 ratio), respectively (dotted lines). **E.** High resolution a-SEC analysis of Xre-RES$^{Pp}_{His6}$ mixed with DNA (S4) in a 1:2 (E) or 1:10 (F) ratio. Chromatograms show elution profiles for Xre-RES$^{Pp}_{His6}$ mixed with DNA. Full lines show 280 nm and dotted lines 260 nm absorbance.

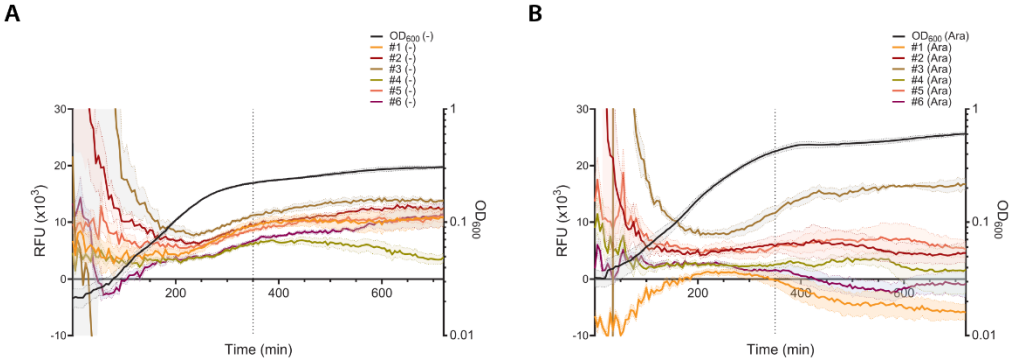

Figure S4. Expression of *xre*^{Pp} alone only partially represses transcription from P_{XR}. Promoter activity measured as GFP relative fluorescence units (RFU) during growth without (**A**, -) or with arabinose (**B**, Ara) for *E. coli* MG1655 containing the promoter reporter pGH254Kgfp::P_{XR}, as well as pBAD33::xre_{opSD}. The curves show mean-of-mean values (line) with SEM (shadow) for the six independent experiments (#1-6). The dotted line indicates the 350 min time point used in **Figure 5A**.

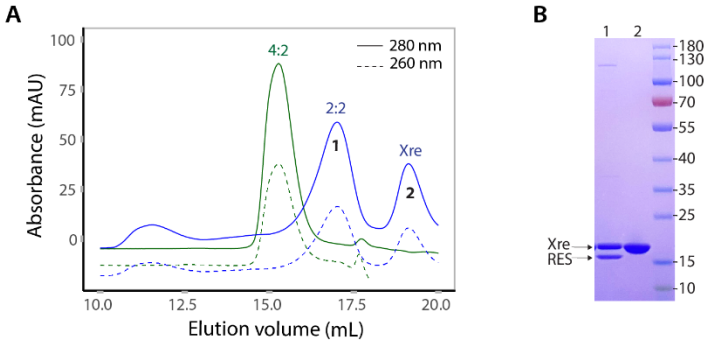

Figure S5. Isolation of the 2:2 Xre-RES^{Pp} complex. **A**. Analytical SEC (a-SEC) analysis. Chromatograms show elution profiles for purified Xre-RES$^{Pp}_{His6}$ (4:2 complex, green) and Xre$_{NHis6}$-RES^{Pp} (2:2 complex and free Xre antitoxin, blue). Full line shows 280 nm absorbance, while dotted line is 260 nm absorbance. **B**. Identity of peak 1 (2:2 complex) and 2 (Xre alone) was confirmed by SDS-PAGE.

Strains	Genotype or description	Source
MG1655	*Escherichia coli* K-12 *rph-1 rfb-1 ilvG*	Laboratory collection
BL21(DE3)	E. coli B F– dcm ompT hsdS(rB– mB–) gal λ(DE3	Agilent
Plasmids		
pUC57::*xre-res*^{Pp}	*P. putida* KT2440 *xre-res* locus including 227bp upstream/60bp downstream	(1)
pBAD33	p15, *araC*, P_{BAD}, Cm^r	(2)
pBAD33::*xre*$_{opSD}$^{Pp}	*P. putida xre* with an optimized Shine-Dalgarno (opSD)[1]	This work
pBAD33::*xre*$_{naSD}$-*res*^{Pp}	*P. putida xre-res* locus with a native SD (naSD)	This work
pGH254K	Mini-R1, *lacZYA* transcriptional fusion vector, Kan^r	(3)
pGH254Kgfp	Mini-R1, *gfp* transcriptional fusion vector, Kan^r	This work
pGH254Kgfp::P_{XR}	Transcriptional fusion of P_{XR}-*xre'* to *gfp*	This work
pGH254Kgfp::P_{XR}Δ1	Deletion of Sequence 1 in P_{XR} (bp 1-34)	This work
pGH254Kgfp::P_{XR}Δ1-2	Deletion of Sequence 1-2 in P_{XR} (bp 1-71)	This work
pGH254Kgfp::P_{XR}Δ1-3	Deletion of Sequence 1-3 in P_{XR} (bp 1-101)	This work
pGH254Kgfp::P_{XR}Δ4	Deletion of Sequence 4 in P_{XR} (bp 107-137)	This work
pGH254Kgfp::P_{XR}Δ3-4	Deletion of Sequence 3-4 in P_{XR} (bp 71-137)	This work
pGH254Kgfp::P_{XR}Δrepeat	Deletion of perfect part of repeat in Sequence 4 in P_{XR} (bp 115-129)	This work
pGH254Kgfp::P_{XR}5'perf	Perfect 5'-repeat in Sequence 4 (substitution G115T)	This work
pGH254Kgfp::P_{XR}3'perf	Perfect 3'-repeat in Sequence 4 (substitution A130C)	This work
pGH254Kgfp::P_{XR}5'flip	Destroyed 5'-repeat in Sequence 4 (113-TTGTCG-118→CGACAA)	This work
pGH254Kgfp::P_{XR}3'flip	Destroyed 3'-repeat in Sequence 4 (129- CGAAAA -134→TTTTCG)	This work
pET-29b(+)	*ori*ColE1, Km^r, T7 promoter	Twist Bioscience
pET-29b(+)::*xre*$_{CHis6}$^{Pp}	*P. putida xre* with a C-terminal His_6-tag	Twist Bioscience
pETDuet-1	Amp^r, *lacI*, T7 promoter	Novagene
pETDuet::*res*$_{NHis6}$-*xre*^{Pp}	*P. putida res* in MCSI, adding N-terminal His_6-tag, and *xre* in MCSII	This work
pETDuet::*xre*$_{NHis6}$-*res*^{Pp}	*P. putida xre* in MCSI, adding N-terminal His_6-tag, and *res* in MCSII	This work

[1]The optimized (op) Shine-Dalgarno (SD) sequence (TAAGGAGGAAATTAA) was included in 5' end of the construct and composed of a strong SD (TAAGGAGG) (4) and additional A's and T's (AAATTAA) to optimize translation.

Tabel S1: Strains and plasmids used in this study. The names of the strains and plasmids are listed together with a genotype or description and the source. Detailed information about the plasmid constructions can be found in **Supplementary Methods**.

References

1. Skjerning RB, Senissar M, Winther KS, Gerdes K, Brodersen DE. 2018. The RES domain toxins of RES-Xre toxin-antitoxin modules induce cell stasis by degrading NAD. Mol Microbiol 0:1–16.
2. Guzman LM, Belin D, Carson MJ, Beckwith J. 1995. Tight regulation, modulation, and high-level expression by vectors containing the arabinose PBAD promoter. J Bacteriol 177:4121–30.
3. Bærentsen RL, Nielsen SV, Skjerning RB, Lyngsø J, Bisiak F, Pedersen JS, Gerdes K, Sørensen MA, Brodersen DE. 2023. Structural basis for kinase inhibition in the tripartite E. coli HipBST toxin-antitoxin system. Elife 12:2022.01.28.478185.
4. Ringquist S, Shinedling S, Barrick D, Green L, Binkley J, Stormo GD, Gold L. 1992. Translation initiation in Escherichia coli: sequences within the ribosome-binding site. Mol Microbiol 6:1219–29.

Oligonucleotide	Sequence (5’-3’)
xre_opSD_Fw	CCCCAGGTACCTAAGGAGGAAATTAAATGCTTGCCGAAGTGCTTCG
xre_Rv	AAAAAGTCGACTCACAGGCCATAGCCCTCG
xre_naSD_Fw	AAAACGGTACCCAAATGCCGAAAAGGAGCATGCC
res_Rv	AAAAAGTCGACCTAGAACAGGCGGCTGTCC
pGH254K_gib_Fw	GATGAACTATACAAATAAATATTATAAAAATTGCCTGATACGCTGCG
pGH254K_gib_Rv	GTTCTTCTCCTTTACTCATAAGCTGTTTCCTGTGTGATAAAGAAAGT
GFPmut2_gib_Fw	TTATCACACAGGAAACAGCTTATGAGTAAAGGAGAAGAACTTTTCACTGGAG
GFPmut2_gib_Rv	TATCAGGCAATTTTTATAATATTTATTTGTATAGTTCATCCATGCCATGTG
pGH254Kgfp_T6613_Fw	AGGAAACAGCTATGAGTAAAGGAG
pGH254Kgfp_T6613_Rv	GTGTGATAAAGAAAGTTAAAATG
PXR_Fw	AACCCGAATTCAGTTTTTGGGGCCGCTTTGC
PXR_Rv	AAAAAGGATCCACCGTTGTCGCGAAGCACTTC
PXRΔS1_Fw	TGGCGGTCAACCTGGCAA
PXRΔS1_Rv	GAATTCAGTTTGTAGAAACGCAAAAAGGC
PXRΔS1-2_Fw	CGACCCGGCAAACTGGCA
PXRΔS1-2_Rv	GAATTCAGTTTGTAGAAACGCAAAAAGGC
PXRΔS1-3_Fw	ATACCGCATACTTGTCGG
PXRΔS1-3_Rv	GAATTCAGTTTGTAGAAACGC
PXRΔS4_Fw	ATGCCATGCTTGCCGAAG
PXRΔS4_Rv	CGGTATATGCCGGGTCATT
PXRΔS3-4_Fw	ATGCCATGCTTGCCGAAGTGC
PXRΔS3-4_Rv	GGCGGTCGAAGCCAGGGC
PXRΔrepeat_Fw	AAAGGAGCATGCCATGCT
PXRΔrepeat_Rv	CAAGTATGCGGTATATGCC
PXR-5’perf_Fw	CCGCATACTTTTCGGCAAATG
PXR-5’perf_Rv	TATATGCCGGGTCATTGC
PXR-3’perf_Fw	CAAATGCCGACAAGGAGCATG
PXR-3’perf_Rv	CCGACAAGTATGCGGTAT
PXR-5’flip_Fw	TACCGCATACCGACAAGCAAATGCCGAAAAGGAG
PXR-5’flip_Rv	TATGCCGGGTCATTGCCA
PXR-3’flip_Fw	CGGCAAATGCTTTTCGGGAGCATGCC
PXR-3’flip_Rv	ACAAGTATGCGGTATATG

res_mcsI_Fw	AAACCGGATCCGTGATTTTGTGGCGAATCAGCG
res_mcsI_Rv	AAAAAGTCGACCTAGAACAGGCGGCTGTCCG
xre_mcsII_Fw	AACCCCATATGATGCTTGCCGAAGTGCTTCG
xre_mcsII_Rv	AAAAACTCGAGTCACAGGCCATAGCCCTCG
xre_mcsI_Fw	AAAAAGGATCCGCTTGCCGAAGTGCTTCGCGAC
xre_mcsI_Rv	AAAAAGTCGACTCACAGGCCATAGCCCTCG
res_mcsII_Fw	AGGGGCATATGATTTTGTGGCGAATCAGCG
res_mcsII_Rv	AAAAACTCGAGCTAGAACAGGCGGCTGTCC
S1_fwd	TTTTTGGGGCCGCTTTGCGGCCCTGGCA
S1_rev	TGCCAGGGCCGCAAAGCGGCCCCAAAAA
S2_fwd	ACCTGGCAAAGCCCTGGCTTCGACCGCC
S2_rev	GGCGGTCGAAGCCAGGGCTTTGCCAGGT
S3_fwd	CGACCCGGCAAACTGGCAATGACCCGGCAT
S3_rev	ATGCCGGGTCATTGCCAGTTTGCCGGGTCG
S4_fwd	CATACTTGTCGGCAAATGCCGAAAAGGAGC
S4_rev	GCTCCTTTTCGGGATTTGCCGACAAGTATG
5'perf_fwd	CATACTTTTCGGCAAATGCCGAAAAGGAGC
S4_5'perf_rev	GCTCCTTTTCGGGATTTGCCGAAAAGTATG
S4_3'perf_fwd	CATACTTGTCGGCAAATGCCGACAAGGAGC
S4_3'perf_rev	GCTCCTTGTCGGGATTTGCCGACAAGTATG
S4_5'flip_fwd	CATAGGCTGTTCCAAATGCCGAAAAGGAGC
S4_5'flip_rev	GCTCCTTTTCGGGATTTGGAACAGCCTATG
S4_3'flip_fwd	CATACTTGTCGGCAAATGGAAAAGCCGAGC
S4_3'flip_rev	GCTCGGCTTTTCGATTTGCCGACAAGTATG

Tabel S2: DNA oligonucleotides used in this study. The table include the names of the oligonucleotides and their DNA sequence.

P_{XR}	AGTTTTTGGGGCCGCTTTGCGGCCCTGGCAATGCTGGCGGTCAACCTGGCAAAGCCCTGGCTTCGACCGCCCGACCCGGCAAACTGGCAATGACCCGGCATATACCGCATA*CTTG*TCGGCAAATGCCGA*AAAG*GAGCATGCCATGCTTGCCGAAGTGCTTCGCGACAACGGT
$P_{XR}\Delta S1$	TGGCGGTCAACCTGGCAAAGCCCTGGCTTCGACCGCCCGACCCGGCAAACTGGCAATGACCCGGCATATACCGCATA*CTTG*TCGGCAAATGCCGA*AAAG*GAGCATGCCATGCTTGCCGAAGTGCTTCGCGACAACGGT
$P_{XR}\Delta S1\text{-}2$	CGACCCGGCAAACTGGCAATGACCCGGCATATACCGCATA*CTTG*TCGGCAAATGCCGA*AAAG*GAGCATGCCATGCTTGCCGAAGTGCTTCGCGACAACGGT
$P_{XR}\Delta S1\text{-}3$	ATACCGCATA*CTTG*TCGGCAAATGCCGA*AAAG*GAGCATGCCATGCTTGCCGAAGTGCTTCGCGACAACGGT
$P_{XR}\Delta S4$	AGTTTTTGGGGCCGCTTTGCGGCCCTGGCAATGCTGGCGGTCAACCTGGCAAAGCCCTGGCTTCGACCGCCCGACCCGGCAAACTGGCAATGACCCGGCATATACCG---ATGCCATGCTTGCCGAAGTGCTTCGCGACAACGGT
$P_{XR}\Delta 3\text{-}4$	AGTTTTTGGGGCCGCTTTGCGGCCCTGGCAATGCTGGCGGTCAACCTGGCAAAGCCCTGGCTTCGACCGCC---ATGCCATGCTTGCCGAAGTGCTTCGCGACAACGGT
$P_{XR}\Delta$repeat	AGTTTTTGGGGCCGCTTTGCGGCCCTGGCAATGCTGGCGGTCAACCTGGCAAAGCCCTGGCTTCGACCGCCCGACCCGGCAAACTGGCAATGACCCGGCATATACCGCATA*CTTG*---*AAAG*GAGCATGCCATGCTTGCCGAAGTGCTTCGCGACAACGGT
P_{XR}-5'perfect	AGTTTTTGGGGCCGCTTTGCGGCCCTGGCAATGCTGGCGGTCAACCTGGCAAAGCCCTGGCTTCGACCGCCCGACCCGGCAAACTGGCAATGACCCGGCATATACCGCATA*CTTT*TCGGCAAATGCCGA*AAAG*GAGCATGCCATGCTTGCCGAAGTGCTTCGCGACAACGGT
P_{XR}-3'perfect	AGTTTTTGGGGCCGCTTTGCGGCCCTGGCAATGCTGGCGGTCAACCTGGCAAAGCCCTGGCTTCGACCGCCCGACCCGGCAAACTGGCAATGACCCGGCATATACCGCATA*CTTG*TCGGCAAATGCCGA*CAAG*GAGCATGCCATGCTTGCCGAAGTGCTTCGCGACAACGGT
P_{XR}-5'flip	AGTTTTTGGGGCCGCTTTGCGGCCCTGGCAATGCTGGCGGTCAACCTGGCAAAGCCCTGGCTTCGACCGCCCGACCCGGCAAACTGGCAATGACCCGGCATATACCGCATACCGACAAGCAAATGCCGA*AAAG*GAGCATGCCATGCTTGCCGAAGTGCTTCGCGACAACGGT
P_{XR}-3'flip	AGTTTTTGGGGCCGCTTTGCGGCCCTGGCAATGCTGGCGGTCAACCTGGCAAAGCCCTGGCTTCGACCGCCCGACCCGGCAAACTGGCAATGACCCGGCATATACCGCATA*CTTG*TCGGCAAATGCTTTTCG*G*GAGCATGCCATGCTTGCCGAAGTGCTTCGCGACAACGGT

Table S3. Promoter DNA sequences. The four repeats in the promoter are indicated by colour (S1, yellow; S2, green; S3, purple; S4, brown) with the repeat underlined and the imperfect palindromic part in italics. Dashes (-) indicate deletions and the start codon of the xre gene is shown with a boldface ATG. Substitutions in relation to the wild type sequence (P_{XR}, top) are shown with red letters.

dsDNA	K_D [M]	SEM	Enthalpy (H) [kJ /mol]	Entropy (-ST) [J/mol]	Free energy (G) [kJ/mol]
S4	$2.31 \cdot 10^{-7}$	$4.61 \cdot 10^{-8}$	-3.35 ± 1.29	-31.8 ± 1.66	-38.4 ± 0.71
5'-perf	$3.41 \cdot 10^{-4}$	$2.64 \cdot 10^{-4}$	-5.36 ± 0.92	-26 ± 2.09	-31.3 ± 1.25
3'-perf	$8.06 \cdot 10^{-5}$	$7.97 \cdot 10^{-5}$	9.14 ± 7.28	-42.9 ± 8.06	-33.8 ± 0.91
3'-flip	NA	NA	NA	NA	NA
5'-flip	NA	NA	NA	NA	NA

Tabel S4. Isothermal Titration Calorimetry (ITC). S4 dsDNA, or variants, was titrated into Xre-RES^{Pp} complex. The calculated binding affinities (K_D), the enthalpy (H), the entropy with temperature (-ST), and the Gibbs free energy (G) are shown. All values are means of three independent replicates with standard error of mean (SEM) indicated. N/A: no binding was observed.